CONVERGENCE ACCELERATION AND SHOCK FITTING FOR TRANSONIC AERODYNAMICS COMPUTATIONS

Mohamed M. Hafez, et al

University of Southern California

Prepared for:

Office of Naval Research

April 1975

UNCLASSIFIED

SECURITY CLASSIFICATION OF THIS PAGE *(When Data Entered)*

REPORT DOCUMENTATION PAGE

READ INSTRUCTIONS BEFORE COMPLETING FORM

1. REPORT NUMBER: USCAE 132	2. GOVT ACCESSION NO.
3. RECIPIENT'S CATALOG NUMBER: AD-A009 898	
4. TITLE *(and Subtitle)*: CONVERGENCE ACCELERATION AND SHOCK FITTING FOR TRANSONIC AERODYNAMICS COMPUTATIONS	5. TYPE OF REPORT & PERIOD COVERED: Technical Report
	6. PERFORMING ORG. REPORT NUMBER
7. AUTHOR(s): Mohamed M. Hafez and H. K. Cheng	8. CONTRACT OR GRANT NUMBER(s): N00014-75-C-0520
9. PERFORMING ORGANIZATION NAME AND ADDRESS: University of Southern California, Department of Aerospace Engineering, Los Angeles, California 90007	10. PROGRAM ELEMENT, PROJECT, TASK AREA & WORK UNIT NUMBERS: "Approved for public release; distribution unlimited".
11. CONTROLLING OFFICE NAME AND ADDRESS: Department of the Navy, Code 438, Office of Naval Research, Arlington, Virginia 22217	12. REPORT DATE: April 1975
	13. NUMBER OF PAGES: 26
14. MONITORING AGENCY NAME & ADDRESS *(if different from Controlling Office)*: Department of the Navy, Code 603, Office on Naval Research Branch Office, 1030 East Green Street, Pasadena, California 91106	15. SECURITY CLASS. *(of this report)*: UNCLASSIFIED
	15a. DECLASSIFICATION/DOWNGRADING SCHEDULE

16. DISTRIBUTION STATEMENT *(of this Report)*

"Approved for public release; distribution unlimited".

17. DISTRIBUTION STATEMENT *(of the abstract entered in Block 20, if different from Report)*

18. SUPPLEMENTARY NOTES

19. KEY WORDS *(Continue on reverse side if necessary and identify by block number)*

Acceleration
Convergence of iterations
Line-relaxation methods
Power method
Nonlinear tranformations
Shock fitting
Transonic small disturbance theory

20. ABSTRACT *(Continue on reverse side if necessary and identify by block number)*

Part One of this report presents a method to accelerate convergence of iterative solutions for elliptic and mixed-type partial differential equations. Part two presents shock-fitting method for the line-relaxation solutions to a transonic potential equation. Significant improvements over existing finite-difference methods in speed (economy) and in accuracy are demonstrated in the framework of transonic small-disturbance theory.

DD FORM 1 JAN 73 1473 EDITION OF 1 NOV 65 IS OBSOLETE

UNCLASSIFIED

SECURITY CLASSIFICATION OF THIS PAGE *(When Data Entered)*

PRICES SUBJECT TO CHANGE

USCAE 132
APRIL 1975

CONVERGENCE ACCELERATION AND SHOCK FITTING FOR TRANSONIC AERODYNAMICS COMPUTATIONS

Mohamed M. Hafez and H. K. Cheng

Office of Naval Research
Contract No. N00014-75-C-0520
Identification Number NR 061-192

Department of Aerospace Engineering
University of Southern California
Los Angeles, California

FORWARD

NR

This report supersedes AIAA Paper 75-51 of the same title, which was presented at the AIAA 13th Aerospace Sciences Meeting, held in Pasadena, California, January 20-22, 1975. Many slips in the original text have been corrected; clarifications on several points, as well as new data, are added in the forms of footnotes, additional figures, and Addenda.

It is believed that the power of the many existing relaxation methods in fluid dynamics can be greatly multiplied with the help of the two techniques under study. Inasmuch as the work may not appear in journal publication form for some time, the distribution of this report will serve a useful purpose.

The research was supported by the Office of Naval Research Fluid Dynamics program under Contract N00014-67-0269-0021, Partial support of M. M. Hafez was also received from NASA Ames Research Center through Ames-University Consortium Agreement NCR-730-501.

CONVERGENCE ACCELERATION AND SHOCK FITTING FOR TRANSONIC AERODYNAMICS COMPUTATIONS

Mohamed M. Hafez and H. K. Cheng
Department of Aerospace Engineering
University of Southern California
Los Angeles, California 90007

ABSTRACT

Two problems in computational fluid dynamics are studied in the context of transonic small-disturbance theory: I. How to speed up the convergence for currently available iterative procedures, II. How a shock-fitting method may be adapted to existing relaxation procedures with minimal alterations in computer programming and storage requirements. The paper contributes to a clarification of error analyses for sequence transformations based on the power method (including also the nonlinear transforms of Aitken, Shanks and Wilkinson), and to developing a cyclic iterative procedure applying the transformations. Examples testing the procedure for a model Dirichlet problem and for a transonic airfoil problem show that savings in computer time by a factor of three to five is generally possible, depending on accuracy requirements and the particular iterative procedure used. A shock-fitting method, valid whether the shock is nearly normal or oblique, is developed; its relation to, and differences from, Murman's shock-point operator (SPO) method are delineated. Improvement over shock-capturing and SPO methods through shock fitting are demonstrated by solutions to an airfoil problem using same mesh sizes.

I. INTRODUCTION

Many current methods of fluid dynamics computations make use of relaxation procedures. There are two aspects of the computation which considerably limit the usefulness and potentiality of these programs: One is the low rate of convergence with respect to iterations, hence costly computer time; the other is the loss of the sharp definition of a shock surface in finite-difference solutions where shocks are "captured." This paper will present studies on these two aspects mainly in the context of the (inviscid) transonic small-disturbance theory. Our study will focus on: I. How to speed up convergence for currently available iterative procedures, and II. How a shock-fitting method may be adapted to existing relaxation programs --- with minimal alterations in computer programming and storage requirements.†

It is quite apparent that similar treatments, the acceleration techniques in particular, can be adopted to speed up convergence of iterative solutions to large algebraic systems arising from other problem formulations (the discretized solutions to integral-differential equations, and the problem via finite-element methods, as well as to certain false-time unsteady problems); this will be explored in separate works.

Need of Acceleration

To see the need of acceleration techniques, we may take as an example the finite-difference solution to Dirichlet's problem in a unit square domain. The speed and storage capacity of the modern computers are simply not high enough for solving this problem to an acceptable accuracy directly by Cramer's rule, nor efficiently by the Gauss elimination method.[1,2] Established relaxation methods, such as iterative procedures of Jacobi (J), Gauss-Seidel (GS), Successive Over-Relaxation (SOR), Line Successive Over-Relaxation (lineSOR) Symmetric Successive Over-Relaxation (SSOR), etc., prove to remain as the reliable way to solve this and other elliptic problems, using modern computers.[2,3,4] The convergence rate of any of these iterative procedures will depend on the magnitude of the eigen value of the largest modulus of the iterative matrix, called spectral radius, denoted here by $|\lambda_1|$. The error of the solution at the k^{th} iterations is, in most cases, gauged by[2-5] $|\lambda_1|^k$.

The need for improvement is apparent from the fact, to be amplified in § 2.3 below, that $|\lambda_1|$ tends to unity as the mesh size vanishes. Thus, for an accurate solution, the convergence is painfully slow. (For certain well-ordered sparse matrices with constant coefficients, the use of direct method can be quite efficient; see Refs. 6 and 7, also 10).

The relative merits for adopting different relaxation procedures may be assessed on the basis of $1-|\lambda_1|$. Lomax and Steger[8] recently discussed possible improvement of convergence characteristics from this viewpoint, which will depend, of course, on certain a priori knowledge of the iterative matrix or the spectral radius. The approach from this viewpoint will not be fully explored here, although the following study does bring out certain important effects of the procedure changes on convergence rate. Instead of altering the basic relaxation procedure (for each iteration), we will adopt a cyclic iterative procedure; (weakly nonlinear) sequence transformations closely related to those of Shanks and Aitken are applied at the conclusion of each cycle, generating initial data (closer to the convergence limit) for the next cycle.

The theoretical basis of our transformations lies in the stipulated properties of the first few dominant eigenvalues of the iterative matrix, similar to that of the power method;[9,3,4] but special allowance is made that moduli of successive eigen values can be very close to each other and to unity. This allowance, we believe, has removed the most (unrealistic) serious limitation of the classical theory of the power method as applied to iterative difference solutions. The error estimates, hence the convergence rates, are established for both first-order and higher-order transforms. The study also clarifies an erroneous notion about the accuracy of Aitken's δ^2-process applied to eigen-value problems (see § 2.2).

† Thus, the first question addresses to accelerating convergence with respect to iterations, whereas the second, in effect, is related to convergence with respect to the mesh sizes, since shock fitting permits the use of a coarser grid.

One efficient way to reduce iterations for the relaxation problems of interest is "grid halving"--starting with coarse grids, the grids are refined at subsequent stages of iterations. The techniques, powerfully demonstrated by Jameson and South,[11,12] should be particularly helpful during the development (debugging) stage of such programs. The common problem of slow convergence eventually appears, however, as grids are refined. As is well known,[2] the relative merit and limitations of the grid-halving are a consequence of the effects of the grid size on the spectral radius, hence, the convergence rate, and can be studied as such (cf. §§ 2.3 and 5). To achieve maximum economy, the technique can be used in combination with other methods, although, for some problems related to perturbation analyses (e.g., Ref. 13, p. 16), application of grid-halving may not be straightforward.

Slow Convergence in Transonic Flow Computations

One of the great recent advances in aerodynamics related to relaxation methods is, perhaps, Murman and Cole's calculation of plane transonic flow based on small-disturbance theory using type-dependent difference schemes, which succeeds in capturing the shock in a super-critical flow.[15] Subsequent works extend the analysis to lifting airfoils, axisymmetric bodies, and three-dimensional wings, and to the full compressible potential equations (Refs. 16-19 ; see reviews Refs. 20 and 21, also 22). The computer storage and the number of arithmetical operations required by programs based on these methods are low enough to make the computations possible even for a modest institution. However, the computer time of 400-1,000 iterations required for the more complicated problems may still demand $\frac{1}{2}$ to 2 hours on an IBM 360/44 or 370/158, and 10-40 min. on a CDC-6600. Use of acceleration techniques with savings of computer time by a factor of three or four is certainly worthwhile, especially if one has a great many problems to solve. We point out in this connection that, unlike those of Dirichlet and other well-conditioned model problems[2,3], the iterative matrix of the quasilinear, mixed-flow problem does not lend itself to an a priori determination of its eigenvalues. The proper choice of the relaxation parameter "ω" for the SOR method in this case has been mostly guess work, where room for improvement is ample. In this respect, we note also that the established approach based on an optimum ω will not necessarily lead to the fastest approach to the convergence limit for the SOR procedure --- even for a Dirichlet problem, as subsequent examinations will show (§ 4).

Shock Fitting for Relaxation Solutions

Finite-difference solutions to inviscid compressible flow, with a discontinuous shock surface satisfying the Rankine-Hugoniot relations, have been carried out in the past mostly as one to an unsteady, or the limit of an unsteady, problem.[23, 24] The most successful among the works along this line belong to Moretti and colleagues.[24,25,26] Like the time-dependent method of Yoshihara and Magnus,[27,28] solutions representing the steady limit are physically sound and can be made reasonably accurate but are quite costly to perform. In the line relaxation method of Murman and Cole, the shock is captured as a part of the continuous solution -- owing largely to the numerical viscosity introduced by the difference schemes, but is smeared out over a few grid points.* In fact, the solutions by the line SOR method do not satisfy the shock conservation laws in some cases, and do not agree with the result obtained via the unsteady approach.[27,28] Murman[29] traces the discrepancy to the error from the shock capturing; he discovers a relatively simple technique to implement the original line SOR method, employing a shock-point operator. However, the SPO solution still takes four or more grid points to complete a shock jump, and the accuracy of the method has been demonstrated only for one case which employed an exceedingly fine grid. It is pertinent, therefore, to examine if the alternative, namely, shock fitting, may succeed with a coarser grid. To the best of our knowledge, works on relaxation method with shock fitting do not exist in the literature. We will demonstrate that for the same mesh sizes, shock fitting does represent an improvement over the line SOR (with and without the SPO) in describing an embedded shock. Some small but noticeable differences from Murman's SPO solution[29] remain, however, to be resolved. (cf. § 8.3).

The first part of this paper, §§2-5, will discuss the acceleration technique and related algorithms, with applications to the model elliptic and transonic equations. The second part, §§6-8, presents our study of shock fitting for relaxation solutions to transonic flow. The kinship of our acceleration technique with the Shanks nonlinear transformation[30] and Aitken's δ^2 - process is noteworthy, but their subtle differences are essential; these will be clarified in § 2. The basis of the power method is introduced in § 2.2. To amplify the importance for allowing close spacings between successive eigenvalue moduli and its consequences, we summarize in § 2.3 certain results of Young[2] for a Dirichlet problem. The main theoretical content of our method is presented in § 3 where the errors in the power method are analyzed, and the sequence transforms serving base to our cyclic iterative method are derived. Numerical experiments with the cyclic acceleration and other methods are tested for the model Dirichlet problem in § 4 and applied to the transonic flow problem in § 5. Section 6 describes our shock-fitting procedure, and § 7 discusses relations to Murman's SPO method. Computation results are studied in § 8.

PART I

2. SEQUENCE TRANSFORMS AND POWER METHOD

2.1 Transformation of Sequence

Use of transformations to improve convergence characteristics of sequences is not unfamiliar in the literature of fluid mechanics and applied mathematics.[34-37] One class of these which bears a kinship to the key equations of our method is the nonlinear transformations of Daniel Shanks,[30] and the related Padé rational fractions.[38] From a sequence, say, $\phi_1, \phi_2, \cdots, \phi_{k-1}, \phi_k, \phi_{k+1}, \cdots$, the transformation gives a new sequence closer to the limit ϕ. The simplest among these is the e_1 transform of Shanks

$$\phi'_{k+1} = \frac{\phi_{k-1}\phi_{k+1} - \phi_k^2}{\phi_{k-1} - 2\phi_k + \phi_{k+1}} \qquad (2.1)$$

* Since the central-difference scheme for the subcritical region does not give precisely the same viscous coefficient, computed shock structure, if obtainable, will be qualitatively different from that in a Navier-Stokes solution.

which predicts the limit ϕ from three successive iterates ϕ_{k-1}, ϕ_k, and ϕ_{k+1}. Equation (2) has been found and applied independently in many earlier works, and the algorithm is often referred to as Aitken's δ^2-process (see Refs. 4, 5, 30-32), which could also be viewed as a derivative-free variant of Newton's method or the method of false position (see for example, Ref. 5, pp. 96-109).*

As a predictor of the limit ϕ for an iterative solution to a nonlinear scalar equation $\phi_{k+1} = g(\phi_k)$, Eq. (2.1) is subject to an error comparable to the square of $\epsilon_k \equiv \phi_k - \phi$ under a nonvanishing $g'(\phi)$, and is, in fact, exact if the equation is linear. However, for the iterative matrix equations of interest (see below), these estimates are not strictly correct even in the linear case. The validity (and accuracy) of Eq. (2.1) and similar transforms must be established on an entirely different basis. Formally, the first-order transform in the present method, Eq. (3.6) below, could be regarded as a varient from that of Aitken and Shanks, Eq. (2.1); however, a point-by-point application of Eq. (2.1) to the iterative solution of a matrix equation proves to be unreliable and uneconomical. (See §§ 3 and 5 below; neither Aitken nor Wilkinson have found their transforms very successful with matrix solutions.) We note in passing that Wilkinson,[4] following Aitken,[32], applied Eq. (2.1) to approximate the lowest-order eigenvector of a matrix, and claimed an $\|\epsilon_k\|^2$ accuracy; but the proof (which overlooks the contribution from the third eigenvectors, Ref. 4, p. 578) is itself in error.

Considering the sequence $\{\phi_k\}$ as the k-term partial sum of a series of an analytic function, Shanks identifies one of his transformed sequence $\{e_n(\phi_k)\}$, to which $\{e_1(\phi_k)\}$ of Eq. (2.1) belongs, with the n^{th} row in the upper triangle of the Padé Table.[30,38] (For Padé' fractions and further relations to Shanks' transforms, see Refs. 39, 40, and 41.) An important observation motivating the work of Shanks is that the transformed sequence $\{e_n(\phi_k)\}$ represents (exactly) the limit ϕ of a sequence $\{\phi_k\}$, if ϕ_k has (precisely) the transient behavior for successive k

$$\phi_k = \phi + \sum_{i=1}^{n} a_i q_i^k \tag{2.2}$$

where a_i and q_i are constants. It is apparent that convergence requires $|q_i| < 1$ and that, for a sequence from the partial sum of a geometric series ($a_i = 0, i \neq 1$), the e_1 transform of Shanks yields the exact limit.† The stipulated exponential transient, Eq. (2.2), is not a general one, for there is no apparent reason that the iterates of a general scalar equation cannot approach its limit algebraically instead. Interestingly, for the iterative solution to a matrix equation, a transient similar to Eq. (2.2) does apply to each component of the solution near the convergence limit (cf. §§ 2 and 3)—a point not fully amplified (recognized) by Shanks. In this respect, the present and Shanks' works could be considered to have come from the same vein.

It is instructive to explore the consequence of the transient assumed in Eq. (2.2). The equation is applied to $k+1$, $k+2$, ..., $k+n$ in addition to k, the resulting system can be used to express the limit ϕ, as well as the n values of $a_i q_i^k$ in terms of ϕ_k, ϕ_{k+1}, ..., ϕ_{k+n} and q_i's,

$$\phi = \sum_{i=0}^{n} C_i \phi_{i+k} \Big/ \sum_{i=0}^{n} C_i \tag{2.3}$$

where C_i is simply the co-factor of ϕ_{k+i} in the determinant

$$\begin{vmatrix} \phi_k & 1 & 1 & \cdots & 1 \\ \phi_{k+1} & q_1 & q_2 & \cdots & q_n \\ \vdots & \vdots & \vdots & & \vdots \\ \phi_{k+n} & q_1^n & q_2^n & \cdots & q_n^n \end{vmatrix}. \tag{2.3a}$$

Since C_i's are independent of k, it can be eliminated by applying Eq. (2.3) n times with k replaced by $k-1$, $k-2$, ..., $k-n$. This leads to precisely the e_n transform of $\{\phi_k\}$.

2.2 Linearized System and Power Method

In the relaxation solution to the difference equations of interest, the unknown ϕ and its k^{th} iterates ϕ_k are vectors with components as many as the number of total grid points N. The iterative matrix equation of interest is

$$\phi_{k+1} = g(\phi_k) \tag{2.4}$$

where the function g depends on the difference equations and the iterative procedure used. In approaching the convergence limit, the error vector

$$\epsilon_k = \phi_k - \phi \tag{2.5}$$

satisfies a linearized matrix equation

$$\epsilon_{k+1} = Q\,\epsilon_k \tag{2.6}$$

where Q is the Jacobian matrix of g, with a remainder comparable to the square of (some norm of) ϵ_k, assuming that g is well-behaved and independent of k. It may suffice, therefore, to analyze the error vector on the basis of this linear recursion relation, with a second-order accuracy. The equations governing the limit solution ϕ may, however, be nonlinear.

We note in passing that Eq. (2.6) is equivalent to a discrete version of a time-dependent system, say,

$$C\,\dot{\varphi} = A\,\varphi \tag{2.7a}$$

for arbitrary matrices C and A, and time step Δt so long as

$$Q = exp.\{\Delta t\, C^{-1} A\}. \tag{2.7b}$$

Conversely, solutions to a discretized time-dependent problem may be considered near the equilibrium limit as the iterative solution to a linear system, Eq. (2.7). Thus, Varga[3] discusses extensively iterative difference methods for elliptic equations, along with forward, backward and Crank-Nicholson schemes for parabolic equations, and interprets the latter as Padé Approximants of the exponential matrix, Eq. (2.7b). (Also see Lomax and Steger's review, Ref. 8.) Here lies the potentiality of the techniques under study for speeding up computations of steady flows using a pseudo-unsteady approach.

Returning to the linear iterative system, Eq. (2.6), the matrix Q has generally a set of eigenvalues λ_i with corresponding eigen vector v_i

$$Q\,v_i = \lambda_i v_i, \quad i = 1, 2, 3, 4, \cdots \tag{2.8}$$

We assume for the moment that the λ_i's are distinct and can be ordered according to their moduli as $|\lambda_1| > |\lambda_2| > |\lambda_3| > \cdots > |\lambda_{N-1}| > |\lambda_N|$. The error

*Aitken also studied successive transformations of new sequences, i.e., e_1^m, cf. Refs. 31 & 32.
†Refer to Addendum A.1, p. 16.

vector of the initial data may then be represented by

$$\epsilon_0 = \phi_0 - \phi_i = \sum_{i=1}^{N} \alpha_i v_i \qquad (2.9)$$

Repeated iterations on Eq. (2.9) with Eq. (2.6) yields the error vector at the k^{th} iteration

$$\epsilon_k = \phi_k - \phi = \sum_{i=1}^{N} \alpha_i v_i \lambda_i^k . \qquad (2.10)$$

This is the main base for the power method of Fadeev and Fadeeva[9,1,3,4] Obviously, convergence requires $|\lambda_i| < 1$ and, near the limit, the error vector is dominated by the lowest eigenvector v_1 as

$$\epsilon_k = \alpha_1 v_1 \lambda_1^k + O(\alpha_2 v_2 \lambda_2^k). \qquad (2.11)$$

Omitting the remainder proportional to λ_2^k, Eq. (2.11) can be applied to three successive iterates and recovers readily the Aitken-Shanks transform, Eq. (2.1). This should not be surprising, because, for $n < N$, and writing q_i as λ_i, the "transient" of Shanks, Eq. (2.2), for which the e_n transform gives the exact limit, is identifiable with the first n terms of the error vector in Eq. (2.10). In other words, the e_n transform applied to matrix solutions finds a theoretical basis in the power method, with an error expected to be proportional to

$$(\lambda_{n+1})^k \ll 1 . \qquad (2.12)$$

Although the approach to the limit is exponential in k, according to Eq. (2.10), $|\lambda_1|$, $|\lambda_2|$, etc., are very close to unity in most problems of interest. This makes the convergence extremely slow; it also makes the error estimates for the e_n transform, Eqs. (2.11) and (2.12), unreliable (see § 3 below). To illustrate this behavior of λ_i's and their dependence on the mesh size, we shall examine below a model elliptic problem.

2.3 Eigen Values of Iterative Matrix: Model Problem

Consider the finite-difference relaxation solution to the Laplace equation in a rectangular domain with ϕ prescribed on the boundary (a two-dimensional Dirichlet problem). Using a uniform mesh size, the length of two sides of the rectangle are taken to be I and J units, respectively, with $I \geq J$. The iterative matrix equation of $N = (I-1)\cdot(J-1)$ unknowns resulting from the central-difference scheme, using standard iterative techniques, can be written as

$$\phi_{k+1} = Q \phi_k + d \qquad (2.13)$$

consistent with Eq. (2.6). The set of eigenvalues of Q is a two-parameter family depending on the iterative procedure used. Following Young[2], the eigen value is denoted by μ_{pq} for the Jacobi (J) method, and by λ_{pq} for the Gauss-Seidel (GS) method. It can be shown that (Ref. 2, pp. 71-73, 131)

$$\lambda_{pq} = \mu_{pq}^2 = \frac{1}{4}\left[\cos\left(\frac{p\pi}{I}\right) + \sin\left(\frac{q\pi}{J}\right)\right]^2 \qquad (2.14a)$$

with $p = 1, 2, \ldots, I-1$, and $q = 1, 2, \ldots, J-1$. For large I and J, the first few (dominant) eigen values are

$$\lambda_{pq} = \mu_{pq}^2 \sim 1 - \frac{\pi^2}{2}\left[(p/I)^2 + (q/J)^2\right] \qquad (2.14b)$$

In terms of the mesh size $\Delta x = \Delta y = h$, the two largest eigen values for the J method are

$$\mu_1 = \mu_{11} \sim 1 - \tfrac{1}{2}\pi^2 h^2, \quad \mu_2 = \mu_{12} \sim 1 - \frac{5}{4}\pi^2 h^2, \qquad (2.15a)$$

and, for the GS method, are

$$\lambda_1 = \lambda_{11} \sim 1 - \pi^2 h^2, \quad \lambda_2 = \lambda_{12} \sim 1 - \frac{5}{2}\pi^2 h^2. \qquad (2.15b)$$

If $|\lambda_1|^k = e^{k \ln|\lambda_1|}$ is taken as an estimate of norm $\| \epsilon_k \|$, the GS method would then take $1/\pi^2 h^2$ or N/π^2 iterations to reduce $\| \epsilon_k \|$ by a factor of e^{-1}; the corresponding iterations for the J method is $2N/\pi^2$. If the Shanks-Aitken transform can be used, the error norm becomes $|\lambda_2|^k = e^{k \ln|\lambda_2|}$, according to Eq. (2.12); comparing λ_2 with λ_1 and μ_2 with μ_1 in Eq. (2.15), the convergence rate is seen to increase two and a half times in either case. The line-relaxation version of the GS or J method has values of $(1-\lambda_{pq})$ or $(1-\mu_{pq})$ twice of those in Eq. (2.14b), hence will converge twice faster, for λ_{pq} near unity.[2,3]

Over-relaxation applies to J and GS methods or their line relaxation versions, using $\phi_{k+1} = \phi_k + \omega(\phi'_{k+1} - \phi_k)$, increase the convergence rate in the model Dirichlet problem, provided $1 < \omega < 2$. For this and other more general matrix equations, Young shows that an optimum ω exists between 1 and 2 for the SOR method, for which the spectral radius reaches its smallest value with (cf. Ref. 2, p. 172, 173)

$$1 - |\lambda_1| = O(\pi h). \qquad (2.15)$$

This would lead to an order of magnitude saving in iterations; but its possibility will not be stipulated here, because the optimum ω cannot be inferred for the nonlinear problem (for ϕ) of interest, and also because the neighborhood of the optimum ω for which Eq. (2.15) holds is very narrow.

Young also observes that for $0 < \omega < \omega_{opt.}$, the spectral radius decreases monotonically with increasing ω toward $\omega_{opt.}$ (where there is a square-root singularity), and that spectral radius increases linearly as $(\omega - 1)$ for $\omega_{opt.} < \omega < 2$. Except when ω is very close to 2, say $\omega = 2 - O(h^2)$, these observations and Eq. (2.15) indicate that the problem of slow convergence is more serious with the range $0 < \omega < \omega_{opt.}$.

An important feature of the SOR solution to the model Dirichlet problem is that, for $\omega_{opt.} < \omega < 2$, all eigenvalues have the same modulus, i.e., $|\lambda_1| = |\lambda_2| = \ldots = |\lambda_N|$ (Cf. Ref. 2, pp. 203-206.) This shows clearly that the applicability of acceleration techniques based on the power method, Eqs. (2.10) - (2.12), is limited only to

$$\omega < \omega_{opt.} \qquad (2.16)$$

for which the first few eigenvalues are as close to unity as

$$1 - \lambda_i = O(h^2). \qquad (2.17)$$

As noted before, for $\omega_{opt.} < \omega < 2$ the need for acceleration may not be as critical.

3. ERRORS IN THE POWER METHOD AND NONLINEAR TRANSFORMATIONS

For large-scale computations involving very fine grids ($h \ll 1$), the accuracy and convergence rate of the Shanks e_n transform summarized in § 2.2 cannot be regarded as well-based. This is because the very fact that

$$\lambda_1 - 1 = O(h^2) \neq 0, \qquad \lambda_i - \lambda_1 = O(h^2), \qquad (3.1)$$

where $i = 2, 3, \ldots, n \ll N$, brought out in § 2.3 for the model elliptic problem, has not been

allowed for in classical works.[1,3-5,9] This unaccounted fact could change the error estimate for the transforms (cf. Eq. (3.3) below). In the following, we shall establish the transforms from a firmer basis, taking into account Eq. (3.1), including the case with repeated λ_i's.

3.1 First-Order Transform

We shall first consider cases without repeated root for the eigenvalues. For the special case with a single dominant eigenvalue, i.e., $|\lambda_1| > |\lambda_2| \geq |\lambda_3|$ etc., the formal basis for the δ^2-process derived from the power method is usually taken as $\epsilon_{k+1} \simeq \lambda_1 \epsilon_k$. The error of this equation may be studied from the (exact) relation based on Eq. (2.10)

$$\epsilon_{k+1} - \lambda_1 \epsilon_k = \sum_{i=2}^{N} \alpha_i v_i \lambda_i^k (\lambda_i - \lambda_1). \tag{3.2}$$

From this, one may formally predict the limit ϕ from two iterates and λ_1

$$\phi = \phi_k + \frac{\phi_{k+1} - \phi_k}{1 - \lambda_1} - \sum_{i=2}^{N} \alpha_i v_i \lambda_i^k \left(\frac{\lambda_i - \lambda_1}{1 - \lambda_1} \right), \tag{3.3}$$

where the last term gives a remainder at most of the order λ_2^k, under Eq. (3.1). The need for a critical analysis is seen from the appearance of $(1 - \lambda_1)$ as the denominator. Larger errors may thus arise, depending on the method for estimating λ_1.

The simplest way of inferring λ_1 is to determine it from three successive iterates via Eq. (3.2) for a chosen (reference) component of ϕ_k's, say ϕ_k^*, at sufficiently large k

$$\lambda_1 = \lambda_1^* + \Delta \lambda_1 \tag{3.4a}$$

with

$$\lambda_1^* = (\phi_{k+1}^* - \phi_k^*) / (\phi_k^* - \phi_{k-1}^*) \tag{3.4b}$$

$$\Delta\lambda_1 = (\phi_k^* - \phi_{k-1}^*)^{-1} \sum_{i=2}^{N} \alpha_i v_i^* \lambda_i^{k-1} (\lambda_i - \lambda_1)(\lambda_i - 1)$$

$$\sim \frac{\alpha_2 v_2}{\alpha_1 v_1} \left(\frac{\lambda_2}{\lambda_1} \right)^{k-1} \frac{(1 - \lambda_2)(\lambda_2 - \lambda_1)}{(1 - \lambda_1)}. \tag{3.4c}$$

By virtue of the extra factor $(\lambda_2 - \lambda_1) = O(h^1)$, λ_1^* as an estimate for λ_1 should be reasonably accurate. An equivalent estimate, which will have less problems than λ_1^* with rounding error and with the sensitivity to the component chosen for reference, is

$$\bar{\lambda} = \sum |\phi_{k+1} - \phi_k| \Big/ \sum |\phi_k - \phi_{k-1}| \tag{3.5}$$

where $\sum$ signifies the summation over all components. Other implimentations on the λ_1 estimates are discussed in § 3.4 later.

With λ_1 from Eq. (3.4), the limit ϕ may now be predicted as

$$\phi = \phi_k + \frac{\phi_{k+1} - \phi_k}{1 - \lambda_1^*} + \Delta_k \phi \tag{3.6a}$$

with

$$\Delta\phi \simeq \sum_{i=2}^{N} \lambda_i^{k-1} \left(\frac{\lambda_i - \lambda_1}{1 - \lambda_1} \right) \left[\frac{\alpha_i v_i^* \lambda_i (\lambda_i - 1)}{1 - \lambda_1} \cdot \frac{\phi_{k+1} - \phi_k}{\phi_{k+1}^* - \phi_k^*} + \alpha_i v_i \lambda_i \right] = O(\alpha_2 \lambda_2^k), \tag{3.6b}$$

where Eq. (3.1) has been used. Similar estimate of $\Delta_k \phi$ can be obtained if λ_1^* in Eq. (3.6) is replaced by $\bar{\lambda}_1$. The transform based on Eq. (3.6 a), with λ_1^* defined by Eq. (3.4a) or its equivalence, will be referred to as the first-order transform. It cannot be identified with the Aitken-Shanks transform, Eq. (2.1), except at the reference point where λ_1 is computed. (We will point out the relative merit of Eq. (3.6) over the δ^2-process in § 4.) Equations (3 6) confirm the validity of the Aitken-Shanks or the e_1 transform under condition Eq. (3.1) which is more relevant to the present study. The classical derivation of Eq. (3.6) by Lyusternik[42] and by others appeared to be fortuitous, since if the factor $(\lambda_i - \lambda_1)$ were omitted from the estimate of $\Delta\lambda_1$, the error in ϕ would have to be amplified by an order $(1 - \lambda_1)^{-1} = O(h^{-2})$!

3.2 Second- and Higher-Order Transforms

Since complex eigenvalues of a real matrix occur in pairs, one must allow for cases in which two or more eigenvalues are equally dominant, e.g., $|\lambda_1| = |\lambda_2|$, even if they are distinct. The need also arise if $|\lambda_2|$ is too close to $|\lambda_1|$ for the first-order transform to be useful.

We shall look for a transform to replace Eq.(3.6), making use of the first n eigenvectors to filter out the error. We assume that all λ_i's are distinct, although some of their moduli may be equal, for which the Fadeev and Fadeeva result, Eq. (2.10), still holds. For this purpose, we shall introduce a polynomial in λ of degree $n \ll N$, taking $p_n = 1$,

$$P_n(\lambda) = \prod_{j=1}^{n} (\lambda - \lambda_j) = p_0 + p_1 \lambda + \cdots + p_n \lambda^n \tag{3.7}$$

where the second equality defines p_j's as functions of λ_j's. The roots of $P_n(\lambda) = 0$ consist of the whole set of eigenvalues. With this and Eq. (3.7), the Fadeev and Fadeeva result leads to equation reminiscent of the Cayley Hamilton theorem[43]:

$$p_0 \epsilon_k + p_1 \epsilon_{k+1} + p_2 \epsilon_{k+2} + \cdots + p_n \epsilon_{k+n} = \Delta_k p \tag{3.8a}$$

with the remainder

$$\Delta_k p = \sum_{i=1}^{N} \alpha_i v_i \lambda_i^k P_n(\lambda_i). \tag{3.8b}$$

On the basis of Eq. (3.8), we may formally predict the limit ϕ from n successive iterates of the same component as

$$\phi = \phi_k + \frac{\sum_{j=0}^{n} p_j (\phi_{k+j} - \phi_k)}{\sum_{j=0}^{n} p_j} + \delta_k^n \phi \tag{3.9a}$$

with

$$\delta_k^n \phi = -\sum_{i=n+1}^{N} \alpha_i v_i \lambda_i^k P_n(\lambda_i) \Big/ P_n(1) \sim -\alpha_{n+1} v_{n+1} \lambda_{n+1}^k \prod_{j=1}^{n} \left(\frac{\lambda_{n+1} - \lambda_j}{1 - \lambda_j} \right) \tag{3.9b}$$

provided all the p_j's, i.e., λ_j's, are known. As in § 3.1, we may apply Eq. (3.9a) to a single (reference) component, without the remainder but with k replaced by $k-1$, $k-2$, ..., $k-n$. The resultant equations, together with Eq. (3.9a) applied to the same component, give a linear system for estimating p_j's, hence λ_j's. In terms of $\phi_{k-n}^*, \ldots, \phi_{k+n}^*$, the p_j-estimates are very accurate, because the relative error is comparable to

$$\frac{\alpha_{n+1}}{\alpha_1} \frac{v_{n+1}}{v_1} \left(\frac{\lambda_{n+1}}{\lambda_1} \right)^k \frac{P_n(1)}{(\lambda - 1)} P_n(\lambda_{n+1}) = O\left[h^{2n} \left(\frac{\lambda_{n+1}}{\lambda_1} \right)^k \right]$$

Now, with this high accuracy in p_j's, the order of the errors in Eq. (3.9a) due to that from p_j's can be shown to be the same as $\delta_k^n \phi$ under Eq. (3.1)

The convergence limit predicted on the basis of Eq. (3.9a), with p_j's estimated in the above manner or by equivalent methods (cf. § 3.4), will be referred to as the "nth-order transform." Its error, according to Eq. (3.9b) is seen under condition Eq.

(3.1) to remain at

$$|\lambda_{n+1}|^k ,$$

the same as would be anticipated from the classical theory (cf. Eq. (2.12)). There is, of course, an additional error of the order $\|\epsilon_k\|^2 \propto |\lambda_1|^{2k}$, if the original Eq. (2.4) is nonlinear. At the reference point, the n^{th}-order transform is identifiable with the e_n transform of Shanks, if the method of estimating p_j's indicated is strictly followed.

Since the p_j's or λ_j's are constants of the limit, and need not be evaluated for each component in the manner as for the δ^2-process[33,4] or ϵ^2-algorithm[45,46], our n^{th} order transform may be considered as being only weakly nonlinear. Eq. (3.9a) specialized to $n = 2$ was obtained by Wilkinson in Ref. 4 where its error was not analyzed.

3.3 The Case with Repeated Roots

If two or more eigenvalues coincide, Eq. (2.10) of the power method may not be applicable because of the lack of a complete set of independent eigenvectors. Suppose that the m^{th} root of det. Q repeats itself r times and that Q is not diagonalizable.† We may introduce r new vectors v_m, $v_{m+1}, \ldots, v_{m+r}$, with

$$\left.\begin{aligned} (Q-\lambda_m I)^r v_{m+r} &= 0, \\ v_j &= (Q-\lambda_m I) v_{j+1}, \quad m \le j \le m+r-1 \end{aligned}\right\} \quad (3.11)$$

The member of the vector set $v_1, v_2, \ldots, v_N$, including the new vectors, can be shown to be linearly independent.

We may now represent the initial error vector by

$$\epsilon_0 = \sum_{i=1}^{N} \alpha_i v_i = \sum_{i=1}^{N}{}' \alpha_i v_i + \sum_{j=m+1}^{m+r} \alpha_j v_j \quad (3.12)$$

where the first sum $\sum'$ excludes those appearing in the second. Repeated iteration on $\epsilon_{k+1} = Q\epsilon_k$ with ϵ_0 gives

$$\epsilon_k = \sum_{i=1}^{N} \alpha_i v_i \lambda_i^k + \sum_{j=m+1}^{m+r} \alpha_j (Q^k - \lambda_j^k I) v_j \quad (3.13)$$

where the matrix Q can be eliminated from Eq. (3.13) by making use of Eq. (3.11). For the case with a double root ($r = 1$), we have

$$\epsilon_k = \alpha_i v_i \lambda_i^k + \alpha_{m+1} k \lambda_m^{k-1} v_m \quad (3.14)$$

as a basis for studying the effect on the n^{th}-order transform. If $m > n$, the order of the remainder $\delta_k^n \phi$ would change only a little, changing from $\exp\{k \ln|\lambda_{n+1}|\}$ to $\exp\{k \ln k \ln|\lambda_{n+1}|\}$. If one of the dominant eigenvalues is repeated, i.e., if $m \le n$, we find Eq. (3.8) remains unchanged because

$$P_n'(\lambda_m) = 0. \quad (3.15)$$

Therefore, the n^{th} order transform holds for a repeated root. The proof may be extended to $r \ge 2$.

3.4 Implementations

Instead of applying the first-order transform to three successive iterates, one may apply it to ϕ_{k-m}, ϕ_k, and ϕ_{k+m}. In this case, Eq. (3.6) is replaced by

$$\phi = \phi_k + \frac{\phi_{k+m} - \phi_k}{1 - \lambda_i^m} \quad (3.16a)$$

with

$$(\lambda_i^m) \simeq (\lambda_i^m)^* = (\phi_{k+m}^* - \phi_k^*) / (\phi_k^* - \phi_{k-m}^*) \quad (3.16b)$$

where the remainders in ϕ and λ_i^m are the same as in Eqs. (3.6b) and (3.4b) with λ_1 and λ_j replaced by λ_i^m and λ_j^m, except the λ_j in λ_j^k. Interestingly, the first-order transform with an even m is applicable to the case with $\lambda_1 = -\lambda_2$ (even though $|\lambda_1| = |\lambda_2|$), the error of the transform belongs, in this case, to the order λ_3^k. Similarly, the n^{th}-order transform may also be applied to iterates separated by m. Generally, the order of the error in ϕ remains at λ_{n+1}^k under condition Eq. (3.1), independently of m.

A key to the successful application of the first-order transform is the provision of an accurate and reliable estimate for the eigenvalue λ_1. One advantage of using Eq. (3.16) with $m > 1$, is, in fact, the reduction in the sensitivity of the first-order transform, Eq. (3.6), with respect to the error in estimating λ_1. We observe in this regard that not only will any error in λ_1 be amplified by the factor $(1-\lambda_1)^{-2} = O(h^{-2})$ in the transform, but the computed value of λ_1^* varies considerably from component to component during the transient. In addition, there is a serious problem with rounding error in the computation of λ_1^*, since, near the convergence limit, both the numerator and denominator of λ_1^* may not remain large compared with rounding errors in certain computers (IBM 360/44, 370/158, etc.) using single-precision arithmetic. In this regard, the alternative of estimating λ_1 by $\bar{\lambda}_1$ from Eq. (3.5), which possesses a larger numerator and denominator and represents an average among the N components, gives, therefore, a better convergence behavior. Another method for estimating λ_1, which proves to provide even better results is to compute λ_1 as a quotient of two inner product

$$\bar{\bar{\lambda}}_1 = \delta_k^T \delta_{k+1} / \delta_k^T \delta_k \quad (3.17)$$

where δ_k is an N-component vector $\delta_k \equiv \phi_k - \phi_{k-1}$. This estimate for λ_1, whose accuracy is comparably to λ_1^* and $\bar{\lambda}_1$, is not to be confused with the "Rayleigh quotient" $\delta_k^T Q \delta_k / \delta_k^T \delta_k$ which requires $O(N^2)$ multiplications as compared to $O(N)$ for $\bar{\bar{\lambda}}_1$ (see, for example, Ref. 5).

Similar comments apply to the problems of estimating p_j's or λ_j's for the higher-order transform. Estimates of p_0 and p_1 for the second-order transform similar to $\bar{\bar{\lambda}}_1$ can be obtained, for example, from $p_0 \delta_k^T \delta_k + p_1 \delta_k^T \delta_{k+1} + p_2 \delta_k^T \delta_{k+2} = 0$ and similar equations.

3.5 Cyclic Acceleration Method††

The first and higher order transforms, Eqs., (3.6a) and (3.3) can be used to improve the accuracy of the relaxation solution at the conclusion of a large number of iterations, as in Lyusternik's work,[42,4] or to convert $\{\phi_k\}$ to a new sequence closer to the limit.

In the present work, these transforms are used as a part of an iterative algorithm: the procedure consists of several cycles, each of which makes k' (10 to 30) iterations on the (nonlinear) algebraic system; the transformation is applied at the end of each cycle to yield an estimate of the limit, which is used as initial data for the next cycle. The error (norm) is reduced by a factor of $\lambda_{n+1}^{k'}$ at the end of each iterative cycle (which is carried into the coefficient α_2 in the next approximation), the error after σ cycles is $O(\lambda_{n+1}^{k})$, where k is the total iterations $\sigma k'$. (The convergence

†If Q is diagonalizable, Eq. (2.9), and hence Eqs. (2.10) and (3.6a), hold even for repeated roots.

††Recently, Young[57] and Della Torre and Kinsner[58] considered acceleration methods in which the acceleration paramater $1/(1-\lambda_1)$ in Eq. (3.6a) is a constant (independent of the iterative solution) chosen a priori.

rate of the first-order transform is therefore unaffected by the subdivision into cycles.) Similarly, the cyclic application of the n^{th}-order transform over a total k iterations (σ times) will have an error norm of the order λ_{n+1}^{k}.

Figure 1 illustrates the cyclic application of the first-order transform for a single component. The application of the transform at the end of the cycle, say the $k+1$ iterate, requires the value of ϕ_{k+1} (on the disc), and the stored value of the same component from the previous iteration, ϕ_k. If λ_1 is to be determined as λ_1^*, Eq. (3.4b), only the value of the reference component ϕ_{k-1}^* is needed and carried as a single datum (for the entire matrix). If λ_1 is chosen to be $\bar{\lambda}_1$, Eq. (3.5), one can compute $\Sigma|\delta_k|$ and store it as a single datum along with ϕ_k; $\bar{\lambda}_1$ is computed after the whole field of ϕ_{k+1} has been obtained. The use of the $\bar{\bar{\lambda}}_1$, Eq. (3.17), requires storing the whole field of δ_k along with that of ϕ_k. When the second-order transform is used (for predicting ϕ after the $k+n$ iteration), full storage for the two vectors ϕ_k and ϕ_{k+1} are required; additional storage for two vectors δ_{k-1} and δ_k will be needed if inner-product quotient forms for p_0 and p_1 are used. The use of the latter quotient often yields smoother approach to the limit and seems to be worthwhile.

A 2-D transonic program similar to Murman and Cole's[15] takes up typically 100 K for the symmetric airfoil problem using 2500 grid points, and typically 200 K for the more general problem involving lift using 5000 points. Each additional storage of the whole field of ϕ_k or δ_k amounts to adding 10 K -- a relatively small addition indeed. Thus the storage requirement for a general 2-D program using the second-order transforms, even with the more complicated estimates for p_0 and p_1 will not exceed 250 K which is well within the 300-350 K capacity of IBM 370/158 class computers. In this regard, we point out that the iterative program for 3-D potential transonic flows of Ref. 12 requires typically 350 K (or less, an achievement of A. Jameson; See Refs. 47 and 48); the feasibility [illegible] the cyclic acceleration method with the second- or higher-order transform to this and similar programs using CDC 6600 or larger computers remain to be studied.

We observe in passing that if Aitken's δ^2-process is strictly followed for every component, i.e., applying the e_1 transform to every grid point, not only the storage and arithmetic operations are increased but the redundancy and nonuniformity in λ_1 implicitly determined for different components may delay the approach to the limit. It proves to be less effective than the present procedure (cf. § 4 below). (For application of the δ^2 and similar acceleration algorithms in aerodynamics computations, see Refs. 44 a and b.)

Among other acceleration techniques based on a power method with comparable simplicity is one in which the eigen value is shifted by changing the iterative matrix Q to $(1-p)^{-1}(Q-pI)$, where p is a constant.[4] This requires, however, a prior knowledge of the dominant eigen values.

An important recent work of A. Brandt[49] on fast numerical solutions for elliptic equations should be mentioned in this connection. The method, called Multi-Level Adaptive Technique (MLAT), recognizes the critical dependence of the convergence rate on the mesh size and exploits the advantage of coarse grids in two ways: (i) an adaptive discretization according to local need, and (ii) a multi-level iterative procedure in which coarser grids participate in solving equations on the finer grids. The programming work is intricate and complex. The cyclic procedure under study could, nevertheless, be applied to speed up such a program if the need arises.

4. EXPERIMENT WITH DIRICHLET PROBLEM

As a model elliptic problem, we consider relaxation solutions to the Laplace equation with values prescribed on a unit square boundary -- the Dirichlet problem. For this particular problem, there are numerous solution methods which would require much less computer time than those to be considered. But as a study of the cyclic iterative methods, this problem offers an ideal testing ground. For this purpose, it may suffice to consider the special problem

$$\left(\frac{\partial^2}{\partial x^2}+\frac{\partial^2}{\partial y^2}\right)\phi = 0 \qquad (4.1)$$

in $0<x<1$, $0<y<1$, with $\phi = 1$ at $y=1$ and $\phi = 0$ elsewhere on the boundary. With uniform grids, five-point central-difference schemes are used to reduce Eq. (4.1) to a system of algebraic equations. Line successive over-relaxation (line SOR) is used as a basic iterative procedure, with the vertical line (of constant x) sweeping from the left to the right in each iteration. To provide a proper perspective in assessing the acceleration technique, examinations will be made on the influence of the relaxation parameter, reverse sweep, variable mesh size (grid halving), and other procedure controls of the convergence characteristics. †

Effect of Relaxation Parameter

For this study, the mesh size h is taken to be 1/30. Four values of the relaxation parameter in the range of $1<\omega<2$ are used, including $\omega = 1.7037$ which approximates the optimum for the line SLOR method in this case (cf. § 2.3). The convergence history of the iterative solutions at a typical point $x = 2/3$, $y = 1/3$ are shown in Fig. 2. The results confirm that the optimum ω gives the highest convergence rate. The solutions for $\omega = 1.6$ and $\omega = 1$ approach the limit monotonically and the case with $\omega = 1.9 > \omega_{opt.}$ exhibits oscillatory behavior, consistent with properties noted in § 2.3. The case with $\omega = 1$ has the slowest approach -- a one percent accuracy is attained only after 300 iterations. Also included are results of reverse sweep applied to the case $\omega = 1.9$, and an acceleration procedure in which Aitken's δ^2-process is followed for each component (at each grid point). The reverse sweep in the case is the line version of the SSOR; for a symmetric iterative matrix as in the model problem under study, its application will give real eigenvalues for the resultant matrix.[3] The nonoscillatory approach for $\omega = 1.9$ with the reverse sweep shown confirms this observation. The δ^2-process applied cyclically to the case with $\omega = 1$ does accelerate the convergence, achieving one percent accuracy after 100 iterations. But the process is less effective than that proposed owing to the redundancy (and inconsistency) in the λ_1 estimate (cf. § 3.5).

Reverse and Horizontal Sweeps for $\omega < \omega_{opt}$

Unlike the case $\omega > \omega_{opt}$, reverse sweep for $\omega < \omega_{opt}$ reduces the convergence rate. The result obtained for $\omega = 1.6$ (not shown) confirms that, for 1% accuracy, reverse sweep with vertical line increases the iterations 5-7 times.

† Cf. Addendum A.2 for similar results for a nine-point difference scheme.

If, instead, a horizontal line is used in the sweep, the reverse (up and down) sweeps worsen the convergence rate but slightly. We note in this connection that the horizontal line version of the SSOR for $\omega = 1.6$ converges even faster than line SOR at the optimum ω (achieving one percent accuracy at $k = 25$, compared with $k = 45$ for the line SOR at optimum ω). The gain through using the "horizontal" line in this case may be attributed to the fact that the non-zero boundary value of ϕ is prescribed along the horizontal line $y = 1$ in this particular problem. Substantial reduction in iterations through use of horizontal line has been found also in study with the transonic small-disturbance flow problem where the main flow and the airfoil are aligned horizontally. However, the SOR and SSOR with horizontal lines do not appear to be very helpful in problems involving imbedded supercritical flow, and will not be pursued in the paper.

Test of Cyclic Acceleration Method: First Order Transform

As a test of the acceleration technique, we apply the proposed cyclic method to the Dirichlet problem for the unit square, using a mesh size of $h = 1/32$. The convergence history for the accelerated solution ϕ at a typical point $x = 10h$, $y = 22h$, is compared with the accelerated Line SOR solution in Fig. 3(a) for a relaxation parameter $\omega = 1.4$, and in Fig. 3(b) for $\omega = 1$. The accelerated line relaxation method (ALSOR) uses the cyclic procedure based on the first-order transform with $m = 2$, cf. Eqs. (3.6a) and (3.16b), implemented by the summation-quotient estimate $\bar{\lambda}_1$ for λ_1, cf. Eq. (3.5). The iteration begins with $\phi = 0$ as initial data for the field, the first cycle begins at $k = 10$, and the cycle is repeated every $= 14$. The effectiveness of the acceleration technique in reducing iterations (and computing time) is obvious from the results shown. In the case of $\omega = 1.4$, the accelerated solution needs only 45 iterations to converge to 10^{-3} from the limit and 70 iterations for 10^{-4}. These are to be compared with 150 and 250 iterations needed in an unaccelerated program with comparable accuracy (cf. Tabulation in Fig. 3(a)). In the case of $\omega = 1$, for which the convergence of the line SOR solution is seen earlier to be very slow, the improvement by the cyclic iterative method displayed in Fig. 3(b) is even more pronounced.

We note in passing that, in appropriate circumstance, this acceleration technique applied to a given $\omega < \omega_{opt.}$ may be competitive or even better than mere changing to the optimum ω (without acceleration). This fact is supported by experiment (not shown) with acceleration of line SOR for $\omega = 1.6$. We point out, in passing, that even though use of reverse sweeps may decrease the convergence rate, acceleration of a line SSOR program via the first-order transform will be generally successful. In fact, in our earlier study (Ref. 50, Figs. 1 and 2), we find the cyclic application of the first-order transform greatly improved the convergence rate, even without constantly updating λ_1 with iterations.

Test of Second-Order Transform. Comparison with Grid Halving.

Figure 4 presents the convergence history of iterative solutions for the same grid point ($x = 10h$, $y = 22h$) using two variants of the second order transform (the full and the dash-dot curves). The uniform mesh size h and the relaxation parameter ω are the same as in Fig. 3(a). The coefficients p_0 and p_1 of the transform, Eq. (3.9a), are estimated by a linear average method over the entire field analogous to $\bar{\lambda}_1$. The full curve is generated by the cyclic method using the transform with $m = 2$ (§3.4), and the dash-dot curve with $m = 1$.

For the Dirichlet problem in a unit square using uniform mesh h, the line (group) version of the J method has eigen values (Ref. 2, p. 453)

$$\mu_{pq} = \cos(q\pi h) \Big/ \left[2 - \cos(p\pi h)\right] \sim 1 - \tfrac{1}{2}(p^2+q^2)\pi^2 h^2 + O(h^4), \qquad (4.1)$$

with p, $q = 1, 2, \ldots, (h^{-1}-1)$. The second and the third dominant eigenvalues differ only in $O(h^4)$, thus, are very close to each other. The line version of the SOR method, i.e., line SOR method, will correspondingly have closely spaced λ_2 and λ_3 (cf. Ref. 2, pp. 173-451). Therefore, the second-order transform, whose remainder is $O(\lambda_3^k)$, cannot be expected to render a significant improvement in this case over the first-order transform whose remainder is $O(\lambda_2^k)$. The results obtained here will be considered as an experiment with second-order transform to the line SOR to be more gainfully applied later. In spite of the lack of a theoretical basis for its superiority in the present application, the result based on the second-order transform with $m = 2$ turns out to converge slightly faster than the corresponding first-order result in Fig. 3(a).

Successive mesh refinement, or grid-halving, provides great saving in computer time, not only because halving the mesh size would require four times the iterations for the same accuracy (unless $\omega = \omega_{opt.}$), but the calculation per cycle on each new mesh (for a 2-D problem) will be four times as expensive as the previous one. In studying the acceleration technique, it is therefore essential to make appropriate comparison with the savings achievable through grid-halving.

The curve in short dash in figure 4 presents the convergence history for ϕ_k by the line SOR method employing grid-halving. The computation starts with one interior grid point where ϕ_0 is set equal to zero. The iterative cycle corresponding to each mesh size h_i is given h_i^{-1} iterations before changing to the finer grid (without waiting for full convergence), except for the cycle with the finest grid $h = (32)^{-1}$, for which the iteration number is not restricted. This choice of the iteration numbers appears to be much more efficient than what had been practiced in published works (cf. Ref. 11, Table 1). For $k < 30$, where the grid-halving has not reached its final cycle, the curve ϕ_k vs. k for grid-halving (without acceleration) appears to be somewhat closer to the limit than the best of our accelerated line SOR solution (based on the second-order transform without grid-halving). But the error in the grid-halving solution becomes larger than the accelerated solutions after the former passes into its final cycle with the finest mesh, as is apparent from the graph and the table.

Thus the required iterations for an accelerated line SOR solution are comparable to, or even less than, an unaccelerated one with grid-halving. How-

ever, depending on the error allowed, there can be considerable saving by grid-halving in the computer time on account of the great reduction in the grid points, hence the computer work, for the coarser grids. If, on the other hand, the deviation from the (estimated) convergence limit is not to exceed 10^{-5} (comparable to the $\Delta\varphi_{max}$ set in Ref. 11), the total computer time for accelerated solution may then be less than that with grid halving. In any case, the acceleration technique can be expected to reduce the computer time for the last stage of the grid-halving with the demonstrated efficiency.†

5. ACCELERATING THE LINE SOR SOLUTION: TRANSONIC FLOW

The partial differential equation governing steady transonic flow is nonlinear and belongs to the mixed (elliptic-hyperbolic) type. Unlike the model Dirichlet problem of §4 the matrix Q governing the error vector is not a priori known; it is not easy to identify, in this case, the optimum relaxation parameter for the efficient use of the SOR method. Application of cyclic acceleration technique to speed up the line SOR method is, therefore, appropriate. The following will study its effectiveness in the context of the transonic small-disturbance theory.

5.1 The Transonic Small-Disturbance Equations: Basic Line Relaxation Program

The steady inviscid plane flow past a thin airfoil near sonic speed can be described by a perturbation velocity potential ϕ satisfying a small disturbance equation, first derived by von Kármán.[51] Let (x,y) be Cartesian coordinates with the x-axis parallel to the free stream, and c_* be a reference length taken below to be the half chord. The upper and lower airfoil surface will be represented as $y = \tau c_* Y(x/c_*, \alpha/\tau, \pm 0)$, where τ is the thickness ratio, and α the angle of attack. In most computational work, Kármán's equations and the boundary conditions have been written in the form, following Cole[52]

$$\left(K_c - (\gamma+1)\widetilde{\Phi}_{\tilde{x}}\right)\widetilde{\Phi}_{\tilde{x}\tilde{x}} + \widetilde{\Phi}_{\tilde{y}\tilde{y}} = 0 \; ; \qquad (5.1a)$$

$$\widetilde{\Phi}_{\tilde{y}}(\tilde{x}, \pm 0) = Y'(\tilde{x}, \alpha/\tau, \pm 0), \quad |\tilde{x}| \le 1 ; \qquad (5.1b)$$

$$\frac{\partial}{\partial \tilde{x}}\left[\!\left[\widetilde{\Phi}(\tilde{x}, \pm 0)\right]\!\right] = 0, \quad |\tilde{x}| > 1 . \qquad (5.1c)$$

$$\widetilde{\Phi}_{\tilde{x}}, \widetilde{\Phi}_{\tilde{y}} \to 0, \quad \text{as } \tilde{x}^2 + \tilde{y}^2 \to \infty . \qquad (5.1d)$$

where $\tilde{x} \equiv x/c_*$, $\tilde{y} \equiv (M_\infty^2\tau)^{1/3} y/c_*$, $\widetilde{\Phi} \equiv (M_\infty/\tau)^{2/3}\phi/Uc_*$, ϕ is the potential jump, and

$$K_c \equiv (1 - M_\infty^2)/(M_\infty^2\tau)^{2/3} . \qquad (5.2)$$

At the trailing edge which is assumed to be sharp, the Kutta-Joukowski condition is to be enforced. The pressure coefficient can be evaluated as

$$C_p \equiv (p - p_\infty)/\tfrac{1}{2}\rho_\infty U^2 = -2\left(\frac{\tau}{M_\infty}\right)^{2/3}\widetilde{\Phi}_{\tilde{x}} . \qquad (5.3)$$

The relative error in this small-disturbance formulation is comparable to C_p, i.e. to $\tau^{2/3}$. For a supercritical flow, the elliptic and hyperbolic regions are separated by the sonic boundary $K_c - (\gamma+1)\widetilde{\Phi}_{\tilde{x}} = 0$, and by the shock $\tilde{x} = \tilde{x}^D(\tilde{y})$ satisfying approximate jump conditions

$$\pm\left\langle -K_c + (\gamma+1)\widetilde{\Phi}_{\tilde{x}}\right\rangle^{\frac{1}{2}} = \left[\!\left[\widetilde{\Phi}_{\tilde{x}}\right]\!\right] \Big/ \left[\!\left[\widetilde{\Phi}_{\tilde{x}}\right]\!\right] = -d\tilde{x}^D/d\tilde{y} \qquad (5.4)$$

where $[\![\ ]\!]$ and $\langle\ \rangle$ signify the jump and the average of quantities in question across the shock, respectively.

Although it is not the best for studying similitude, Cole's form, Eqs. (5.1) - (5.3), will be adopted below for the convenience in making comparison with works of Murman and others.[15,16,29] (To eliminate $(\gamma+1)$ from Eq. (5.1a) one can simply replace all M_∞ by $(\gamma+1)^{1/2} M_\infty$ in Eq. (5.1) - (5.3), except in $(1 - M_\infty^2)$ of Eq. (5.2).)

In setting up the numerical procedure, the far-field condition Eq. (5.1d) is replaced by one over a rectangular boundary $\tilde{x} = \pm 3$, $\tilde{y} = \pm 6$, with $\widetilde{\Phi}$ satisfying the far-field behavior consistent with Eqs. (5.1). For a symmetric airfoil, the $\tilde{x}$-axis can be used in place of the lower boundary $\tilde{y} = -6$. In the cases of a high subsonic free stream (i.e. $K_c > 0$) to be analyzed below, the $\widetilde{\Phi}$ value over the far boundary can be described by that based on the linearized form of (5.1a) for a vortex and doublet of unknown strengths, to be determined in the course of the iteration. The vortex strength, i.e. the circulation, is directly related to the potential jump at the trailing edge; the doublet strength depends on the airfoil thickness distribution as well as the near-field nonlinear corrections, and can be estimated from data on the boundary with a least-square method at the end of each iteration. Unlike Krupp and Murman's procedure,[16] the potential jump across the x-axis behind the trailing edge is assumed uniform and kept at the value in the previous iteration until a new potential jump is generated at the trailing edge.

The basic solution procedure, to which the acceleration and shock fitting methods will be applied, follows that of Murman and Cole.[15] A central-difference operator with second-order accuracy is used in the elliptic region, and an implicit backward difference operator with a first-order accuracy is used in the hyperbolic region. In this basic program, a parabolic point operator corresponding to $\widetilde{\Phi}_{\tilde{y}\tilde{y}}$ is used at a grid point between the elliptic and the hyperbolic regions. The difference equations are solved by a line relaxation method, assigning appropriate ω's to the two regions). The unknown at points belonging to the same vertical line are solved simultaneously, while the line sweeps downstream.

In solving the line problem, the matrix is linearized by assigning values to the coefficient of P.D.E. (5.1a) from the previous sweep; the resulting tridiagonal matrix for the line can be readily inverted.

The basic program used in the subsequent studies is written for an IBM 370/158. The grid has 81 points in $\tilde{x}$ and 62 points in $\tilde{y}$ (or 31 points in $\tilde{y}$ if the problem has symmetry in $\tilde{y}$), using unequal but gradually varying mesh size. The finest meshes are assigned over $|\tilde{x}| \le 1$ and $\tilde{y} = \pm 0.02$ where $\Delta\tilde{x} = 0.05$ and $\Delta\tilde{y} = 0.04$ with the mesh sizes increasing outward.

The truncation error in the difference equation system is generally of the order $\Delta\tilde{x}$ and $(\Delta\tilde{y})^2$. There is, however, a re-expansion singularity resulting from a mismatch of streamline and surface curvatures at the shock root where the surface pressure is known to vary like $x' \log x'$, with $x' = \tilde{x} - \tilde{x}^D$, uncovered by Oswatitsch and Zierep[53] (also see Ref. 54). This singularity causes a unit-order error in the difference equation for $\widetilde{\Phi}$ near the

† Refer to A.2 in Addenda for a study of the second-order transform applied to a nine-point central difference procedure.

shock root, but the relative errors in velocities belong to the order $\Delta\tilde{x}\log\Delta\tilde{x}$. (Hence, there is no gain in using a second-order difference scheme near the shock, unless the re-expansion singularity is analytically accounted for.) With this in mind, our solution will be no more accurate than

$$\mathcal{R} = O\left(\Delta_1\tilde{x}\log\Delta\tilde{x},\ \Delta_1\tilde{y}^2\right) \tag{5.5}$$

with $\Delta_1\tilde{x}$ and $\Delta\tilde{y}$ taken to be the smallest $\Delta\tilde{x}$ and $\Delta\tilde{y}$. Test of convergence with respect to grid size indicates nevertheless that the $\Delta\tilde{x}$ dependence may be considerably smaller than $(\Delta\tilde{x}\log\Delta\tilde{x})$ at points removed from the singularity.

5.2 Examples: Circular Arc Airfoil

As a first example for transonic flows, we study the acceleration of the line SOR solution for a circular arc airfoil at zero incidence, for $K_c = 1.8$. The problem considered has a subsonic free stream but has an embedded supersonic region with an interior shock boundary. The same solution has been studied previously by Murman in Ref. 29 and will be analyzed again later for shock fitting in § 8.

The unaccelerated solution is generated by the line SOR program with the smallest mesh being $\Delta\tilde{x} = 0.05$, $\Delta\tilde{y} = 0.04$, using over-relaxation in the subsonic region and under-relaxation in the supersonic region. Cyclic iteration procedures, using the first- as well as the second-order transforms, are applied. Each cycle consists of sixteen iterations ($k' = 16$), with $m = 4$ (cf. § 3.4); the first cycle commences at $k = 9$ for the first-order procedure and $k = 17$ for the second-order procedure. The linear average quotient form $\bar{\lambda}_1$ is used for estimating λ_1, and the inner product form is used for estimating p_0 and p_1 (cf. §§ 3.1 and 3.4). (Linear average forms for estimating p_j's have also been used without major differences.)

The convergence histories of solutions by the three different procedures are illustrated in Fig. 5(a) - 5(c) for $K_c = 1.8$ at $\tilde{x} = -0.025$, $\tilde{y} = 0$, for different combinations of the relaxation parameters ω in the elliptic and hyperbolic regions. In each case, the initial (trial) data are furnished by a sufficiently accurate solution to the same problem at $K_c = 2.1$, corresponding to a lower free-stream Mach number. The unaccelerated line SOR solution is shown as a solid curve; the accelerated solution using the first-order transform (referred to as ALSOR-1 in the figures) is shown as a thin solid curve drawn through data from all iterations ; for the solution accelerated by the second-order transform (referred to as ALSOR-2), only data points at the end of the cycles are shown (in circles).

Figure 5(a) shows $\tilde{\phi}_{\tilde{x}}$ *vs.* the number of iterations k for the case in which $\omega = 1.4$ in the elliptic region and $\omega = 0.9$ in the hyperbolic region. The improvement in the convergence rate through cyclic application of the transforms is obvious. A factor of three to four reduction in the number of iterations is possible, depending on whether the accuracy requirement is set at 10^{-2} or 10^{-3} (cf. the table in Fig. 5(a)). We note that 10^{-2} is comparable to the truncation error of the difference equations; 10^{-3} is therefore a reasonable margin needed for confirming the convergence of the iterative solutions. To approach the limit with the 10^{-3} accuracy, the unaccelerated solution will require 350 or more iterations.

Figure 5(b) gives the results for a different pair of relaxation parameter: $\omega = 1.8$ in the elliptic region and $\omega = 0.8$ in the hyperbolic region. This combination turns out to give a much better convergence behavior. The line SOR solution (solid curve) approaches the limit within 10^{-2} at 40 iterations and within 10^{-3} at 80 iterations. The accelerated line SOR using on the first-order (thin solid line with print out marks) requires even less work: 18 iterations for 10^{-2} and 45 iterations for 10^{-3}. (We note that this set of calculations used a shorter cycle than those in (a) and (c) of Fig. 5 with $k' = 8$.) The convergence is so rapid in this case that use of the second-order transform is considered unnecessary.

Most transonic flow computations to date have employed over relaxation in the elliptic region and under relaxation in the hyperbolic region. Figure 5 (c) presents a case with a uniform relaxation parameter, $\omega = 0.95$ for the entire field. With this ω, convergence of the line SOR procedure becomes exceedingly slow -- 400 iterations or more would be needed to approach the limit within 10^{-2}. The power of the cyclic transform method to speed up convergence is most clearly demonstrated in this case. At three levels of accuracy, 10^{-2}, 10^{-3} and 10^{-4}, the accelerated solution using the first-order transform approaches the limit in 65, 120 and 230 iterations, respectively. Application of the second-order transform reduces the iterations further to 30, 60 and 140 (cf. table in Fig. 5(c)).

5.3 Example with Circulation

Satisfactory convergence of the iterative solutions to the 2-D transonic problem involving lift is known to require 250-1200 iterations.[16,19] We shall examine below the convergence characteristics of a line SOR solution and its accelerated version for a circular-arc airfoil at incidence, with $K_c = 2.29$ and $\alpha/\tau = 0.1454$, corresponding to $M_\infty = 0.848$, a 6% thickness ratio, and a $\frac{1}{2}^\circ$ angle of attack. The line SOR procedure uses $\omega = 1.3$ and 0.8 for the subsonic and supersonic regions, respectively. The cyclic acceleration procedure employs the first-order transform with $m = 2$, $k' = 12$ iterations/cycle, and λ_1 being estimated by the inner product form Eq. (3.17). Typical convergence histories for the velocity perturbation on the top and bottom of the airfoil surfaces are shown in Fig. 6(a) for a point near the mid chord, $\tilde{x} = -0.025$ and $\tilde{y} = +0$. The unaccelerated solution is given as a solid curve and the accelerated solution in open circles. For the latter only data points at the conclusion of each cycle are shown. The improvement in convergence rate through the cyclic method is quite evident, although not exceedingly great for this particular point. The usefulness of the method is more clearly shown in Fig. 6(b), where the convergence history for the circulation $\tilde{\Gamma} = [\![\tilde{\phi}]\!]_{T.E.}$ is presented. The accelerated solution approaches the limit within 10^{-3} after 150 iterations, whereas for the same accuracy the line SOR without acceleration takes 800 iterations. Oscillations in $\tilde{\phi}$ of the order 10^{-3} are detected to persist at some grid points. This may be eliminated by using a smaller ω or the second-order transform.

The corresponding C_p distribution over the airfoil (not shown) indicates existence of supercritical flow on both sides of the wing, with a weak shock on the top. The result is comparable to the C_p determined from the wind tunnel experiments of Knechtel.[51] As noted by Krupp and Murman,[16] however, a successful

correlation of computer solutions with the experimental data from Ref. 55 and other sources has to depend on a departure from Eqs. (5.2) and (5.3) in computing K_c and C_p (using instead, $K_c=(1-M_\infty^2)M_\infty^{-1}\tau^{-2/3}$, and $C_p=-2\tau^{2/3}M_\infty^{-2/3}\tilde{\phi}_{\tilde{x}}$). This ambiguity (though slight) can be settled only after adequate studies are made on the basis of the second-order small-disturbance theory, and a systematic analysis of errors in wind-tunnel experiments. We prefer to examine this question in a separate work, which is not relevant to the present study.

As a transition to the second part of our study, namely, shock fitting, we observe in passing that the shock jumps deduced from the converged solutions in all preceding examples, as in many solutions based on current SOR programs, do not fully satisfy the Rankine-Hugoniot relation Eq. (5.4). This discrepancy can be easily detected by comparing the arithmetical means of the surface speed with the normal shock value $\langle \tilde{\phi}_{\tilde{x}} \rangle = K_c/(\gamma+1)$ which is required at the root of the shock. In the last example considered, the shock strength is found to be 20% too low.†

PART II

6. SHOCK FITTING APPLIED TO LINE SOR

6.1 Preliminary Remarks

Aside from the inadequacy in predicting shock jumps, the line SOR procedure following the Murman-Cole scheme may also give an excessively thick transition zone for an oblique shock. This can be illustrated by an application of the procedure to a linear supersonic wedge flow, for which only the backward-difference operator needs to be used and no iteration is required. Figure 7 presents the profile of $\tilde{\phi}_{\tilde{x}}$ at different $\tilde{y}$-levels computed with $\Delta\tilde{x}=\Delta\tilde{y}=10^{-1}$ in the region $0\le\tilde{x}\le 1.05$ $0\le\tilde{y}\le 1.05$ above the wedge and behind the shock discontinuity. While the exact solution gives $\tilde{\phi}_{\tilde{x}}=-1(\tilde{x}-\tilde{y})$, where $1(\xi)$ is a step function in ξ, the computed solution takes 10 grids at $\tilde{y}=0.45$, and 20 grids at $\tilde{y}=1.05$, to complete the transition. This model suggests that solutions for sonic boom and for shock-interaction studies by the line SOR methods should, perhaps, be taken with caution in the supersonic range, although the nonlinear steepening, absent from the model, could place a limit on the shock thickness. In any case, the model solution confirms the validity of the common practice of defining the shock position by the point of maximum slope for $-\tilde{\phi}_{\tilde{x}}$ or C_p, noting that such a point (in circle) is reasonably close to the exact oblique shock location at each level, in spite of the excessively large shock thickness. We observe that the SPO (shock-point operator) of Ref. 29 does not apply to a shock with a supersonic-supersonic transition (cf. § 7), therefore the solution using SPO in this case may give a relatively large transition zone compared to that in a supersonic-subsonic transition, unless a very fine grid is used. The good agreement of the SPO solution with Magnus[28] in the bow shock location may be attributed partly perhaps to the useful definition of the shock position mentioned.

The lack of a sharp definition for the shock discontinuity in the line SOR solution may obliterate the re-expansion singularity,[53,54] the sonic-line/shock intersection,[21,54] and other fine details of an embedded supersonic flow region, although descriptions of some of these features could be improved with a very fine local grid, at least in principle.

Whereas the jumps in the SPO solution follow the shock polar rather closely,[29] the solution requires a very fine grid with a mesh size 10^{-3} of the wing chord, as noted earlier. The agreement appears to be less satisfactory in regions where the shock is not nearly normal (cf. points f and g in Fig 6 of Ref. 29). In the following, shock fitting will be adapted to implement the line SOR procedure of Murman and Cole; results comparable with Murman's can be obtained with much coarser grids.

6.2 Basic Procedure

The Shock Polar

The Rankine-Hugoniot relations in the transonic small-disturbance theory have been given earlier in Eq. (5.4), and are repeated here for convenience

$$\langle -K_c+(\gamma+1)\tilde{\phi}_{\tilde{x}}\rangle=\frac{[\![\tilde{\phi}_{\tilde{y}}]\!]^2}{[\![\tilde{\phi}_{\tilde{x}}]\!]^2}\,, \tag{6.1}$$

$$[\![\tilde{\phi}_{\tilde{y}}]\!]/[\![\tilde{\phi}_{\tilde{x}}]\!]=-\left(\frac{d\tilde{x}^D}{d\tilde{y}}\right). \tag{6.2}$$

With $\tilde{u}=\tilde{\phi}_{\tilde{x}}$, $\tilde{v}=\tilde{\phi}_{\tilde{y}}$, the first equation is identified with the shock polar in the hodograph $\tilde{u}$-$\tilde{v}$ plane. The second equation signifies the continuity of the tangential velocity component across the shock $\tilde{x}=\tilde{x}^D(\tilde{y})$. The latter may be replaced by the continuity of $\tilde{\phi}$ across the shock

$$[\![\tilde{\phi}]\!]=0 \tag{6.3}$$

which assures the existence of an intersection of the $\tilde{\phi}$ surfaces belonging to two sides of the shock. The ridge where the two surfaces meet, therefore, locates the shock boundary. However, the slope change at the intersection has to satisfy the shock polar Eq. (6.1) or

$$\langle -K_c+(\gamma+1)\tilde{\phi}_{\tilde{x}}\rangle=\left(d\tilde{x}^D/d\tilde{y}\right)^2 \tag{6.4}$$

An essential point to observe is that each oblique Rankine-Hugoniot shock in the physical plane belongs to a point on the shock polar Eq. (6.1), and that the image of a surface of discontinuity in the hodograph plane, which does not conserve the tangential momentum, cannot coincide with the shock polar (except perhaps at their intersections). It follows that a solution with shock boundary which satisfies Eq. (6.1) will also conserve tangential velocity and potential, i.e., satisfying Eqs. (6.2) and (6.3).†† This will be substantiated by the numerical experiment.

In comparing the computed shock jump with the shock polar, it is convenient to eliminate the non-uniform upstream condition from Eq. (6.1). This can be accomplished by letting $K_c^*=(K_c-(\gamma+1)\tilde{\phi}_{\tilde{x}})^*$

$$\left.\begin{aligned}\bar{u}_2&\equiv(\gamma+1)\cdot[\![\tilde{\phi}_{\tilde{x}}]\!]/(-K_c^*)\\ \bar{v}_2&\equiv\left(\tfrac{3}{-K_c^*}\right)^{3/2}\left(\tfrac{\gamma+1}{4}\right)\cdot\left|[\![\tilde{\phi}_{\tilde{y}}]\!]\right|\end{aligned}\right\} \tag{6.5}$$

The shock polar Eq. (6.1) may then be reduced to a single curve[29]

$$27\,(2+\bar{u}_2)\,\bar{u}_2^2-32\,\bar{v}_2^2=0\,. \tag{6.6}$$

† Use of finer grids does not prove to be helpful.

†† If $\kappa[\![\tilde{\phi}_{\tilde{y}}]\!]/[\![\tilde{\phi}_{\tilde{x}}]\!]=-d\tilde{x}^D/d\tilde{y}$, then Eq. (6.6) becomes $27\,(2+\bar{u}_2)\,\bar{u}_2^2-32\,\kappa\,\bar{v}_2^2=0$.

Treatment of Points Around Shock

The line-relaxation procedure to which the shock fitting method will be applied is basically that of Murman and Cole described in § 5. The modifications in the difference equations are found mainly in the treatment of the grid point on each horizontal line nearest to the shock on the downstream side, and the nearest grid point along each vertical on the upstream side, labelled as P, S, and Q, respectively, in Fig. 8. Three types of local shock inclination must be distinguished in treating point P, depending on where the shock crosses the vertical through P (cf. Fig. 8):

(a) a point between P and the nearest grid above P, i.e., a backward inclination;

(b) a point between P and the nearest grid below P, i.e., a forward inclination;

(c) a point beyond the nearest grid.

The inclination in (c) can be either forward or backward and includes the locally normal shock. This classification, as well as the introduction of points P and Q, are necessary in order to describe the shock boundary as one with a slope discontinuity for the $\tilde{\phi}$ surface. †

At point P, the difference equation in the original line SOR procedure is replaced by the difference form of the shock-polar equation Eq. (6.1). In all cases, the $\tilde{\phi}_{\tilde{x}}$'s are evaluated from the central differences at points A and B, and $\tilde{\phi}_{\tilde{y}}$'s from the differences at D and C, in the manner shown in (a), (b) and (c) of Fig. 8. The splitting of the calculation for the $\tilde{\phi}_{\tilde{y}}$ - jump into two parts along different vertical lines is a crucial feature which retains the shock as a surface of discontinuity. The original difference equation for the upstream point Q is also in need of implementation in cases (a) and (b), because one of the five points in the backward hyperbolic operator has been lost to the other side of the shock. The needed datum is supplied by forward (downstream) extrapolation to P from three upstream points.

The Modified Line SOR Procedure

The foregoing treatment, together with the hyperbolic, elliptic, and parabolic difference operators and other minor implementations applied to other interior points, complete the difference-equation system.

If the flow at P is subsonic, data at grids to the left (upstream) of P are known from the most recent sweep, and those to the right, as well as the R.H.S. of Eq. (6.1), are taken from the previous iteration; Eq. (6.1) then determines ϕ at P. This results in two (linearized) tridiagonal matrix equations for the lines above and below the shock, which may be readily inverted for each sweep.

If the shock has a supersonic downstream, both point P and its downstream point S have to be treated (cf. Fig. 8.A). Continuity of ϕ across the shock as well as interpolation along vertical line are used for determining ϕ at P and the points below. The shock equation (6.1) is applied to determine ϕ at S. ††

Relocating the Shock and Sonic Boundaries

The sonic and shock boundaries are relocated before the next iteration. This step is important for a consistent treatment of the elliptic and hyperbolic points. For this purpose, the central difference form of $\tilde{\phi}_{\tilde{x}}$ is computed for the region of interest from stored $\tilde{\phi}$ data acquired from the recent sweep. The sonic point is identified with

$$K_c' \equiv K_c - (\gamma+1)\,\tilde{\phi}_{\tilde{x}} = 0. \qquad (6.7)$$

This will relocate the boundary "RSHC" of Fig. 9, separating the hypersonic and elliptic regions, which includes the portion of the shock ("SR" in Fig. 9) with a subsonic downstream. A criterion is used to distinguish the shock from the sonic curve (for a shock, the decrease in $\tilde{\phi}_{\tilde{x}}$ across the "sonic point" is required to be no less than $5\Delta\tilde{x}$).

The shock position can be alternatively located by the intersection of the $\tilde{\phi}$-surfaces belonging to the upstream and downstream side of the shock (located in the previous interation). This should also locate the portion of shock ("ST" in Fig. 9) which has a supersonic downstream, provided numerical viscosity will not smear out the gradients of $\tilde{\phi}$ near the shock. For problems invoiving embedded supersonic regions in general, and the example to be studied in particular, the shock strength over the portion "ST" is rather weak and its extent is very narrow. A sub-routine to apply shock-fitting to this part of the flow region has not been made to date.

Accuracy and Local Grid Refinement

The shock-fitting solution permits the use of a grid coarser than that used in SPO and other relaxation procedure for comparable accuracy. This is because the several (4 or more) grid points making up the artificial shock structure can be eliminated. This may mean an order of magnitude, or more, saving in the computing time. Even with shock fitting, however, the relatively coarser grid must still be sufficiently refined near the shock for a clearer definition of the shock location and an adequate description of the re-expansion singularity. Since the finer grid is required only around the shock, relaxation solution with the finer grid needs to be carried out only in a smaller (rectangular) domain enclosing the shock, with boundary value for $\tilde{\phi}$ taken from the solution for the coarser grid. The local grid refinement in this manner may, therefore, be made without increasing the dimension of the iterative matrix.

7. RELATION TO SHOCK-POINT-OPERATOR METHOD

In certain subtle aspects, the shock-fitting method presented in § 6 and the SPO method of Murman[29] are strikingly similar. It must be emphasized again that the SPO method generates its solutions by continuous calculation as in the original Murman and Cole procedure (a shock jump is completed in four or more grid points). As such, it is not relevant (and unfair) to assess the SPO right next to the "shock point". The following will delineate these similarities as well as their differences, which are helpful for interpreting the results in § 8.

† Refer Addendum A.3 for more general consideration.
†† Refer Addendum A.4 for more detailed description.

7.1 The Shock-Point Operator

The elegant device of Murman in Ref.29 is simply to replace the parabolic operator in the original procedure(at a supersonic-subsonic transition point)by one in which the original difference operator is changed to the sum of the x-differences in an elliptic and a hyperbolic operators. Using the lettered subscripts to denote points shown in Fig. 10, the equation written for $\varphi \equiv -(1+1)^{-1} K_c \tilde{x} + \tilde{\Phi}$, is

$$\frac{(\varphi_{\tilde{x}})_B^2 - (\varphi_{\tilde{x}})_I^2}{2\,\Delta\tilde{x}} + \frac{(\varphi_{\tilde{x}})_I^2 - (\varphi_{\tilde{x}})_A^2}{2\,\Delta\tilde{x}} = \frac{(\varphi_{\tilde{y}})_D - (\varphi_{\tilde{y}})_C}{\Delta\tilde{y}} \quad (7.1)$$

where, to be sure, $(\varphi_{\tilde{x}})_I$ is supposedly the value of $\varphi_{\tilde{x}}$ in a concinuous solution at the intermediate (or imaginary) point between (the two mid points) A and B (cf. Fig. 10). This value $(\varphi_{\tilde{x}})$ is of course not needed in the computation, in which the equation for the shock-point P can be written as

$$-K_c + \left(\tfrac{1+1}{2}\right)\cdot\left[(\tilde{\Phi}_{\tilde{x}})_A + (\tilde{\Phi}_{\tilde{x}})_B\right] = -\frac{\Delta\tilde{x}}{\Delta\tilde{y}}\cdot\left[(\tilde{\Phi}_{\tilde{y}})_D - (\tilde{\Phi}_{\tilde{y}})_C\right]\left[(\tilde{\Phi}_{\tilde{x}})_B - (\tilde{\Phi}_{\tilde{x}})_A\right]^{-1} \quad (7.2)$$

Formally, the shock-point operator Eq. (7.2) could be identified with the shock polar Eq. (6.1) in difference form, provided that the mesh ratio $\Delta\tilde{x}/\Delta\tilde{y}$ can be taken as the shock slope $d\tilde{x}^D/d\tilde{y}$, and that the shock point P lies on the shock. In such a case,

$$(\tilde{\Phi}_{\tilde{y}})_D - (\tilde{\Phi}_{\tilde{y}})_C = (\tilde{\Phi}_e - \tilde{\Phi}_p)/\Delta\tilde{y} - (\tilde{\Phi}_p - \tilde{\Phi}_f)/\Delta\tilde{y} = [\![\tilde{\Phi}_{\tilde{y}}]\!] . \quad (7.3)$$

For a plane normal shock, the SPO will indeed agree with the shock condition Eq. (6.1), irrespective of the mesh ratio and the other stipulation because the transverse velocity $\tilde{\Phi}_{\tilde{y}}$ vanishes.

In general, Eq. (6.1)and (7.2) for P do not agree. Thus the correct shock transition cannot be accomplished in a single jump by the SPO itself; but the correct jump can be completed in a few (say four or more) grid points in a relaxation solution utilizing the SPO algorithm, as demonstrated by Murman.[29] Murman is able to show theoretically in Ref. 29 that difference equations based on the hyperbolic and elliptic operators, making use of Eq. (7.1) or (7.2) at shock points, do reproduce correctly the correct jumps connecting flow upstream and downstream, which are many grid points away from the plane oblique shock (under the stipulation that the plane oblique shock passes through two grid points, i.e. $d\tilde{x}^D/d\tilde{y} = \Delta\tilde{x}/N\,\Delta\tilde{y}$, where N is an integer).

It is apparent that the way in which the shock is captured by the procedure using SPO will be quite similar to that by the Murman and Cole and other methods based on continuous calculations — a few grid points have to be spent to arrive at the correct jump.

Aside from the fact that it is not easy to have $\Delta\tilde{x}/\Delta\tilde{y} = N\,d\tilde{x}^D/d\tilde{y}$, the other fact which prevents the SPO from yielding the right jump at the shock point is that the difference in $\tilde{\Phi}_{\tilde{y}}$ on the R.H.S. of Eq. (7.2) is computed from data at e, p, and f along the same vertical line (cf. Fig. 10 (a) and (b)). It is quite apparent from the illustration in Fig. 10 (b) that $\tilde{\Phi}_{\tilde{y}}$ at D will be under-estimated by the SPO in most cases.

Had $(\tilde{\Phi}_{\tilde{y}})_D$ been evaluated along the next vertical to the left of point P, as in (a) or (b) in Fig. 8, (and if the scale ratio could also be properly chosen) the SPO would have become a shock-fitting scheme. The splitting in the $[\![\tilde{\Phi}_{\tilde{y}}]\!]$ calculation represents a fundamental difference of the shock fitting from the SPO procedure.

7.2 SPO as an Elliptic Operator Fitted to a Shock

In problems with embedded supersonic flow, the shocks often appear nearly normal to the free stream with $d\tilde{x}^D/d\tilde{y}$, $(\tilde{\Phi}_{\tilde{y}})_D$ and $(\tilde{\Phi}_{\tilde{y}})_C$ being numerically small. This would suggest that the R.H.S.'s of both Eqs. (6.1) and (7.2) could be omitted, and the two equations would then become equivalent. Namely,

$$\langle -K_c + (1+1)\,\tilde{\Phi}_{\tilde{x}} \rangle = -K_c + \left(\tfrac{1+1}{2}\right)\cdot\left((\tilde{\Phi}_{\tilde{x}})_A + (\tilde{\Phi}_{\tilde{x}})_B\right) = 0, \quad (7.4)$$

implying a normal shock. This stipulation is misleading, however, because over the part of the shock farther from the airfoil, although $d\tilde{x}^D/d\tilde{y}$ is small (say, 1/4 to 1/16), both upstream and downstream value of $-K_c + (1+1)\,\tilde{\Phi}_{\tilde{x}}$ may also be small. A more penetrating interpretation, which relates SPO to the shock fitting as well as the notion of a normal shock, is to consider the SPO as an elliptic operator at P fitted locally to a model shock. This model shock, though oblique and curved, obeys everywhere the normal shock condition

$$\langle -K_c + (1+1)\,\tilde{\Phi}_{\tilde{x}} \rangle = 0. \quad (7.5)$$

This equivalence may be seen as follows.

The elliptic difference operator of the small-disturbance equation applied to P is

$$\left\{K_c - \tfrac{1+1}{2}\left[(\tilde{\Phi}_{\tilde{x}})_B + (\tilde{\Phi}_{\tilde{x}})_I\right]\right\}\cdot\left[(\tilde{\Phi}_{\tilde{x}})_B - (\tilde{\Phi}_{\tilde{x}})_I\right] = + \frac{\Delta\tilde{x}}{\Delta\tilde{y}}\left[(\tilde{\Phi}_{\tilde{y}})_D - (\tilde{\Phi}_{\tilde{y}})_C\right], \quad (7.6)$$

where the central-difference quotients are used and the letter subscript I refers to the mid point in Fig. 10 (a) but the value $(\tilde{\Phi}_{\tilde{x}})_I$ represents the value $\tilde{\Phi}_{\tilde{x}}$ continued analytically from behind the shock (if point I happens to lie on the upstream side). To first-order accuracy in $\Delta\tilde{x}$, this value can be computed from Eq. (7.5) as

$$(\tilde{\Phi}_{\tilde{x}})_I = 2K_c - (1+1)(\tilde{\Phi}_{\tilde{x}})_A . \quad (7.7)$$

Substituting Eq. (7.7) into Eq. (7.6) we recover precisely the SPO, Eq. (7.2).

Hence, the SPO solution should agree with the solution generated by the shock-fitting program described in § 6 , provided the term $(d\tilde{x}^D/d\tilde{y})^2$ or $[\![\tilde{\Phi}_{\tilde{y}}]\!]^2$ is completely turned-off from Eq.(6.4) or (6.1), as if for a normal shock. This latter version of shock-fitting may be referred to as "normal-shock-fitting" (NSF) for the lack of a better term. This equivalence may explain the success of the SPO in greatly reducing the number of grid points for shock transition.

As an algorithm, there is nevertheless difference between the NSF scheme and the SPO. For, in SPO, the shock point P is an elliptic point and the point corresponding to the first one after the

jump is point 1. In the NSF, however, the point P (cf. Fig. 8) carries the information from the Hugoniot relation Eq. (6.1), and the first elliptic point lies farther downstream from P. In other words, the elliptic point in the SPO is one grid farther upstream from that in the NSF. The first jumps after a "shock" recorded in the SPO and NSF will accordingly be different. (This will also depend on the method with which the gradient of the potential is deduced.) Since this jump does not satisfy the conservation law, the NSF solution, like the SPO solution, will rely on numerical dissipative terms inherent in the difference equations to bring about the correct transition (in a few grid points). Interestingly, the proof given in Ref. 29 for the consistency of the SPO solution with the conservation laws for an oblique shock over a rectangle (with a base large compared to $\Delta\tilde{x}$) may be readily extended to the NSF solution.

8. NUMERICAL STUDY WITH SHOCK FITTING AND SPO METHODS

8.1 Comparison of Shock Fitting with SPO Solutions

In order to bring out clearly the difference of the solution using shock fitting from other treatments, we shall compare solutions from computer programs based on three methods of treating the shock :

(i) Shock fitting (cf. § 6);
(ii) Shock-point operator (cf. § 7.1);
(iii) Continuous calculation, i.e., shock-capturing (§§ 5.1 and 6.2)

The basic computer programs used in (i) and (ii) are the same as in (iii). Program (ii) is essentially Murman's "Fully Conservative" (FCR) program but will be referred to here simply as the SPO program. We point out that, because of the differences in certain details in their basic SOR programs, a direct comparison of the shock-fitting solution from program (i) with Murman's SPO result of Ref. 29 may not reveal very clearly the changes due to the different treatments of the shock. A program based on the NSF procedure (§ 7.2) was also made in our earlier study. But its difference from the SPO program (ii) is too slight to warrant its inclusion in the comparison.

The problem analyzed in detail is that of the symmetric circular arc airfoil at $K_c = 1.8$ studied previously in § 5.2, which features an embedded supersonic region terminated by a shock.† Most results to be presented below are obtained for the grid with $\Delta\tilde{x} = 0.0125$ and $\Delta\tilde{y} = 0.01333$ near the airfoil which will be seen to be adequate for describing the rapid pressure variation associated with the re-expansion singularity mentioned before. We note that this grid is considerably coarser than the finest uniform grid used by Murman in Ref. 29, which has $\Delta\tilde{x} = 0.002$, and $\Delta\tilde{y} \simeq 0.008$ (corresponding to $\Delta x = 0.001$, and $\Delta y \simeq 0.004$). Thus the smallest $\Delta\tilde{x}$ and $\Delta\tilde{y}$ used here are 6.25 and 1.5 times the corresponding meshes used in Ref. 29.

The line SOR program using shock-fitting is applied to this grid over a small rectangle $0 < \tilde{x} < 1$, $0 < \tilde{y} < 0.59$ enclosing the shock in a manner described in § 7.1. The solutions generated from the basic line SOR program provides the initial data (trial solution); in the shock fitting study, SPO solutions have also been used as initial data to determine the improvement gained . The number of grid points is kept the same as in our basic SOR program (iii) for the larger 6 × 6 rectangle, i.e. 81 × 31 points. Iterative solutions for programs (i) - (iii) all converge satisfactorily in 100 - 200 iterations (without the help of acceleration techniques). The additional computer time needed for shock fitting in the examples considered is comparable to that for the basic program. (The number of grid points used in the corresponding SPO calculation of Ref. 29 is about 3 times larger, but with a rectangular domain half the size of ours. The computer work required for a converged solution may presumably be 6 times longer.)

8.2 Study of Results

Comparison with Shock Polar

A critical test for the adequacy of the numerical solutions in describing the shock is to compare them with the shock polar in the hodograph plane. This is examined in (a) and (b) of Fig. 11 for the SPO and the shock-fitting solutions, respectively, generated for the same grid $\Delta\tilde{x} = 0.0125$, $\Delta\tilde{y} = 0.0133$. The points $(\tilde{u}, \tilde{v})$ in Fig. 11 (a) designated by a given symbol correspond to successive grid points along a given distance from the airfoil, i. e. a constant $\tilde{y}$ (labeled in the box); Eqs. (6.5) are used except that quantities with the "+" superscript are replaced by the local values, and the subscript "2" is omitted. The reference value of K_c is evaluated at a point upstream where the large departure from the smooth solution begins. The number labeled with the data provides the relative grid position in the downstream direction. With one exception, SPO solutions take 4 grid points or more to reach the vicinity of the shock polar (note the flagged symbols), as reported in Ref. 29. However, the agreement varies from fair to poor, indicating that the SPO, for the mesh sizes used, is not effective in describing the inclined part of the shock. In Fig. 11(b), we correlate velocity jumps (circles) computed from $\tilde{\phi}$ data stored at the end of the iteration, using second-order accurate formulae. The agreement with the shock polar clearly illustrates the adequacy of the mesh sizes employed and the improvement by the shock-fitting over the SPO solution (using the same mesh sizes). Also shown are the hodograph data of the SPO solution of Ref. 29 computed with a much finer grid $\Delta\tilde{x} = 0.002$; only data closest to the polar curve are taken from Ref. 29 for comparison.

The data from the shock-fitting solution shown correspond to the range of $0 < \tilde{y} < .2$ with subsonic flow downstream. Extrapolation of the recorded shock data to the point where the downstream is sonic suggests that the sonic boundary intersects the shock between 0.20 and 0.225. An extrapolation of the shock-jump data along with SPO solutions suggests that the shock strength vanishes between $\tilde{y} = 0.2$ and 0.25 . The relative positions of these two points appear to be consistent with the picture envisioned in Fig. 9.

Surface Pressure

To indicate the type of improvement which can be made over the original line SOR solution in surface pressure, we compare in Fig. 12 the solutions generated from the basic program (iii), with $\Delta\tilde{x} = 0.05$ and $\Delta\tilde{y} = 0.04$ (in short dash), and from the SPO program (ii), with $\Delta\tilde{x} = 0.0125$ and $\Delta\tilde{y} = 0.04$ (in solid curve). The shock-fitting

† A slightly supersonic case with a bow shock has also been worked out, Cf. A.6 in Addenda. The study also demonstrates the simultaneous application of acceleration and shock fitting techniques.

solutions with finer grid will be examined more thoroughly, in the subsequent figure. The data presented are sufficient to indicate that appreciable departure from the original SOR solution is expected to occur only in $.45 < \tilde{x} < 0.95$. Again, we observe that the pressure jump at the surface requires 4 grid points to complete. We have also included in this figure some data points inferred from curves presented in Ref. 29 for subsequent reference. These include Murman's line SOR solution with $\Delta\tilde{x} = 0.04$ (in filled circles), Murman's two SPO solutions with $\Delta\tilde{x} = 0.04$ and $\Delta\tilde{x} = 0.002$ (in filled and open triangles). Their data in the shock transition zone are not shown. The two sets of SPO data from Murman correlate very well among themselves, but have a maximum slightly lower than our SPO solution.

The corresponding result from a more refined calculation by our SPO program (ii), using smaller $\tilde{y}$ - mesh, $\Delta\tilde{y} = 0.01333$, is shown in Fig. 13 as a short-dash curve. Its difference from the result with a coarser grid shown previously is very little. In fact, subsequent calculation using an even smaller x-mesh ($\Delta\tilde{x} = 0.00625$, $\Delta\tilde{y} = 0.01333$), shows again very little difference in the surface pressure except for a sharper definition for the shock.

The shock fitting solution with $\Delta\tilde{x} = 0.0125$, $\Delta\tilde{y} = 0.01333$ is shown as a full curve which is quite close to the SPO curve (in short dash). Hence the SPO and shock fitting give essentially the same surface speed, although the SPO with the same grid fails to give an accurate shock jump at points removed from the airfoil surface, as shown previously in Fig. 11.

We note, however, that the SPO result of Murman (included as a long-dash curve) is located farther downstream than our solution (1% chord) with a correspondingly larger shock strength (2%) and a lower maximum for the surface speed (1%).

Sonic/Shock Boundary

Figure 14 presents the sonic/shock boundary from the SPO solution (in short dash) and from the shock fitting solution (in full curve), for the same grid with $\Delta\tilde{x} = 0.0125$ and $\Delta\tilde{y} = 0.01333$. This sonic/shock boundary is inferred from the local sonic condition. The part of the shock boundary for the SPO solution has a spread over 4-5 grid points (not shown). The shock-fitting result appears to follow the short-dash curve of the SPO solution, with a slight but interesting deviation between $\tilde{y} = 0.1$ and $\tilde{y} = 0.225$, the last point is near point S inferred previously to be the intersection of the sonic locus and the shock. There appears to be a slight indentation, along with changes in the curvature sign, at $\tilde{y} = 0.2 - 0.25$, suggesting an intersection involving a small angle between the shock and sonic boundaries at S.

Included in Fig. 14 for comparison are the sonic/shock boundaries based on the basic SOR program (iii) using $\Delta\tilde{x} = 0.05$ and $\Delta\tilde{y} = 0.04$, (in dash-dot curve) and the result inferred from the SPO solution given by Murman[29] using an x-mesh equivalent to $\Delta\tilde{x} = 0.002$ (in dash). The (dash-dot) boundary given by the regular shock-capturing method, believed to be affected little by further grid refinement, is somewhat smaller than our shock-fitting and SPO solutions.

Murman's SPO sonic/shock boundary, on the other hand, extends farther downstream than the shock-fitting result, consistent with the observation made earlier in Fig. 13. Murman's SPO shock curve appears to run parallel to that from the shock fitting below $\tilde{y} = 0.1$; this agreement in shock slope is consistent with the corresponding agreement found in the study with the hodograph shock polar (Fig. 11). The streamwise displacement in Murman's sonic boundary from ours is quite appreciable, being 3% of the wing chord at $\tilde{y} = 0.3$. The discrepancy between our shock-fitting solution and Murman's SPO solution will be examined more critically in 8.3. The above comparisons in Figs. 11-13 suffice to establish that shock fitting provides an improvement over the shock-capturing as well as SPO methods in locating the shock and describing flow details in its vicinity, although little difference is found at the airfoil surface.

In our shock-fitting procedure, the condition for the continuity of the tangential velocity component has not been explicitly used. A sufficient condition for fulfilling this is that the two potential surfaces from upstream and downstream intersect at the shock boundary. A point-by-point examination has been made along the shock. In no case have we found the potential-surface intersection to occur beyond the same grid pair bracketing the velocity discontinuity defining the shock. Fig. 15 demonstrates such a consistency for the level $\tilde{y} = 0.0891$.

8.3 Accuracy and Further Grid Refinement

The discrepancies with Murman's very refined solution[29] brought out above suggest readily that a higher accuracy may be needed for shock fitting than anticipated. This suggestion gains special significance in view of the re-expansion singularity noted earlier.[53,54] The shock-fitting solution is therefore repeated with a finer grid, using $\Delta\tilde{x} = 0.00625$, $\Delta\tilde{y} = 0.01333$. This is about 3 times the $\tilde{x}$-mesh and 1.5 times the $\tilde{y}$-mesh used in Ref. 29. Since the field away from the shock is affected little by shock fitting, rectangular boundary enclosing the main part of a shock smaller than the previous solution is used, with $.4 < \tilde{x} < .9$, $0 < \tilde{y} < .59$. In this way, the total number of unknowns in the difference equations remains the same as before. This result of the grid-halving turns out to give negligible change. Noticeable but very small differences can be found in the shock strength and the surface speed near the shock (refer to fine dots in Fig. 13), and in the shock location near the new vertical boundary $\tilde{x} = 0.4$. The latter deviation could very well result from the inadequate description of the supersonic-supersonic shock transition in the present programs, which may cause difficulty at the boundary which was set too close to the shock. The degree of invariance of the solution with respect to grid refinement shown in the solutions confirmed the accuracy of our shock fitting solution.

Two more sources of error may account for the discrepancies. One may arise from the far-field description used in the procedures, a doublet of an unknown strength has been used in both methods. Nevertheless, the reasonably good agreement with solutions from programs (ii) and (iii) in regions removed from the shock (cf. Figs. 12 and 13) gives

ample evidence that Murman's SPO solution and our shock-fitting solution agree in the far field.

The remaining source of the discrepancies may be traced to the convergence property of the iteration procedures. For the shock-fitting solution, one hundred twenty iterations has been used to approach the convergence limit with changes in $\tilde{\phi}_{\tilde{x}}$ less than 10^{-3} per 20 iterations.† **

9. CONCLUSIONS

In this paper, we have studied techniques of accelerating the relaxation methods and treating a shock discontinuity in the context of the transonic small-disturbance theory.

Essential in the acceleration technique is a transformation applied cyclically to the iterative solutions. The transformation generates a new set of data closer to the convergence limit for iterations in the next cycle. The key formula has much in common with the "e_k" (or "e_m") transform of Shanks,[30] also Aitken's δ^2-process,[31-33] but derives its theoretical basis from the power method.[3,9]

Cyclic techniques using the first- and the second-order transforms have been tested in a model Dirichlet problem and the transonic airfoil problem. The results have demonstrated the effectiveness of the technique in speeding up the convergence of the line relaxation solutions for the elliptic as well as quasi-linear, mixed-type problems, with different choices of the relaxation parameters and sweep directions. In most cases studied, reduction in the total iteration number by a factor of two to four can be achieved, depending on the accuracy requirement and other considerations.

In certain situations, acceleration by the cyclic transform method proves to be as efficient as the practice of successive grid refinement (grid halving) and, in any case, it can be used to speed up the latter's convergence for the finest grid. The method can be adapted easily by existing iterative programs with minor increases in the data storage requirement.

Formulae similar to those of the first- and second-order transforms have been derived by Lyusternik[42] and Wilkinson,[4] which break down however, as the moduli of the dominant eigenvalues of the iterative matrix approach unity. The present study has contributed to a more critical error analysis for the transforms, which allows for a set of closely-spaced eigenvalue moduli to approach unity. Implicit in the transform is the assumption of the existence of dominant eigenvalues whose moduli are larger than those of the rest. Situations do arise wherein this stipulation is not met (e.g., if $\omega > \omega_{opt.}$ in the model Dirichlet problem). This remains a weakness of the method, but may be remedied by readjusting the relaxation parameter, or introducing reverse sweep, in the basic line SOR program.

Applications of the cyclic method have been limited to accelerating the line SOR solutions of Murman and Cole for a circular-arc airfoil at small incidence. The results suggest that similar improvement in convergence properties may be expected for more complicated 2-D and 3-D elliptic or mixed-type problems. This approach also has the potentiality for speeding up certain pseudo-unsteady finite-difference methods.

For treatments of shock discontinuity, we have developed a shock fitting scheme to implement the line SOR solution to the transonic small-disturbance theory. The scheme differs from existing works on shock fittings, which deal with unsteady problems without making use of a velocity potential. The relative simplicity of the algorithm is comparable to the shock-point operator (SPO) of Murman. The study shows that the SPO is consistent, to the first order of $\Delta\tilde{x}$, with an elliptic operator, using a derivative boundary condition (at the left) provided by the Hugoniot condition for a normal shock. In this sense, the SPO can be interpreted as a model case of shock fitting, which perhaps explains the improvement of the SPO over the original shock-capturing method (in terms of the number of grid points required to complete a shock jump).

Numerical experiments with the shock fitting and the SPO have been made for a supercritical flow past a circular-arc airfoil at transonic parameter K_c=1.8 and -1.83. The improvement by the shock fitting over SPO (for the same grid), in satisfying the Hugoniot condition and in defining the shock position, is demonstrated. For solutions with comparable accuracy, the shock fitting should provide an order-of-magnitude saving in computing time. Result for K_c=-1.83 of shock fitting agrees well with the bow-shock solution of Magnus and Yoshihara[27]. The study of acceleration in this case has also demonstrated that acceleration and shock fitting can be applied simultaneously with expected gains in efficiency and accuracy.

ACKNOWLEDGMENTS

The study is supported by the Office of Naval Research Fluid Dynamics Program. We would like to thank Earll M. Murman for helpful discussion and valuable advice. Richard H. Edwards and Milton D. Van Dyke have raised several questions contributing to clarifications in the text. Dr. Van Dyke has also helped in unravelling numerous slips and typo's from the earlier version (AIAA Paper 75-51). To both of them, we express our deep appreciation. The senior author (H.K.C.) would like to acknowledge his discussions earlier with Morton Cooper, ONR, and A. H. Van Tyle, NOL, who motivated our work on the acceleration techniques.

Acknowledgment is due to Garry Tee, Ahmed Namoury and Sen-yih Meng for their assistance in the study, and to Elizabeth Harris and Gail Wamsley in the typing and production of the report.

Partial support of M. M. Hafez from NASA Ames Research Center through Ames University Consortium is also acknowledged.

ADDENDA

A.1 Relations to Geometric Series and Remarks on Anti-Limit (p. 3)

More generally, the $e_n\{\phi_k\}$ yields the exact limit, if ϕ_k can be represented by the k-term partial sums of n geometric series.

In this work we have not explored the potentiality of Shanks' transformation to convert a divergent

†Cf. Addendum A.5 for further comment on differences from Murman's (Ref. 29) results.

**Cf. Addendum A.6 for the study of the slightly supersonic (K_c<0) case and of acceleration of line SOR with shock fitting.

procedure to a convergent one, corresponding to Shanks' notion of an "anti-limit." This fact may be quite useful; for example, if $|\lambda_1| > 1$ but $|\lambda_i| < 1$, $i = 2, 3, \ldots, N$, Eq. (3.6a) still holds.

A.2 Accelerating Line SOR Based on a 9-Point Difference Scheme (p. 7)

Numerical experiments with our acceleration technique have been made on line SOR method using a 9-point difference scheme (cf. Fig. 4.A). In this case, D. Young's[2] theorem for optimum relaxation parameter does not hold, although Garabedian has estimated the optimum ω for point-iterative procedures by studying an associated hyperbolic PDE[56]. The optimum-relaxation parameter is not known for the line SOR procedure considered here. In Fig. 4.A a typical convergence history of the unaccelerated results, using $\Delta x = 1/30$, is shown as a solid curve. The accelerated result based on a second-order transform is shown in short dash with circle, which approaches the limit within one percent in 30 iterations, as compared to 3 or 4 hundred for the unaccelerated one.

A.3 Types of Shock Inclinations Involving Subsonic Downstream (p. 12)

More generally, one must allow for possible situations wherein a shock intersects the vertical at an x-station further downstream than that through P (cf. Fig. 8). The limitation to the three types of inclinations shown in Fig. 8 does not seriously affect the examples computed in our study, including the case with a slightly supersonic free stream. When the situations mentioned do occur, the grid point for the elliptic operator above (or below) point S would be lost (to the other side of the shock); but the missing $\tilde{\phi}$ data can be furnished by invoking continuity of $\hat{\phi}$ across the shock and interpolation (or extrapolation) along the vertical through point S.

A.4 Shock Fitting in the Case of a Supersonic-Supersonic Transition (p. 12)

If the shock has a supersonic downstream, both point P and its downstream point S have to be treated. The following will discuss the treatment in a line SOR procedure. When the flow region analysed is completely downstream of the "limiting characteristics," the problem may be treated either by the characteristic method or by a difference procedure, using the vertical line sweeping the field only once.

Consider first the treatment in a line-relaxation procedure. If points directly below P are regular points where the hyperbolic operator is applicable, such as in sketch (a) of Fig. 8.A, $\tilde{\phi}$ at P and the unknown $\tilde{\phi}$'s at hyperbolic points below P can be determined in each iteration in terms of the $\tilde{\phi}$ value at the intersection of shock and the vertical through P, using interpolation and invoking continuity of $\tilde{\phi}$ across the shock. The first shock equation, Eq. (6.1), will then be used to determine $\tilde{\phi}$ at point S. The algebraic system for the hyperbolic points directly below point S may then be solved. If the shock in sketch (a) were to intersect the next horizontal line between P' and S', the treatment of point P or P' should then be applied to point S'. The missing information at P' (which is now upstream of the shock) in this case will be supplied by the continuity of $\hat{\phi}$ at the shock via extrapolation. Similar treatment can be applied to shocks with smaller shock angles. Suppose that the slope of the supersonic-supersonic shock $d\tilde{x}^D/d\tilde{y}$ turns out to be large enough (relative to $\Delta\tilde{x}/\Delta\tilde{y}$) so that point "P" occurs directly above the point "S" which belongs to the next lower horizontal, such as the "P'" in sketch (b) of Fig. 8.A. In this case, $\tilde{\phi}$ at P' can be determined directly by interpolation between the shock and the point S below. With a still larger shock angle, there may be two or more grid points between the shock and S along the vertical in sketch (b) of Fig. 8.A. In this case, more extrapolation work along the vertical for $\tilde{\phi}$ (and $\tilde{\phi}_{\tilde{x}}$) will be needed. Clearly, the determination of the type of shock inclination depends on the relative magnitudes of $d\tilde{x}^D/d\tilde{y}$ and $\Delta\tilde{x}/\Delta\tilde{y}$.

If the flow field analysed is thoroughly supersonic downstream of a certain $\tilde{x} = \tilde{x}_s$, for all $\tilde{y}$, a one-sweep procedure marching forward in $\tilde{x}$ can be used. In this case, the algorithm to treat a supersonic-supersonic transition remains basically the same as in the line SOR procedure described in the last paragraph, except that it takes only a single sweep, and that the shock inclination has to be determined from Eq. (6.2) for the next vertical line after completing the computation for each line; an inner (iterative) loop is, however, needed in applying Eq. (6.1) as a cubic equation for $[\![\tilde{\phi}_{\tilde{x}}]\!]$, i.e., for $\tilde{\phi}$ at point S.

A.5 Further Comments on Differences from Murman's SPO Solution for $K_c = 1.8$ (p. 16)

The small difference from Murman's SPO solution for $K_c = 1.8$ (Ref. 29) noted above (1% chord in shock location, 2% in shock strength, and 3% chord in the sonic-boundary displacement) is believed to result from a smaller rectangular domain (in grid refinement) used in Ref. 29.

A.6 Shock Fitting in a Slightly Supersonic ($K_c < 0$) Case: Acceleration of Line SOR with Shock Fitting (pp. 14, 16)

In as much as the limited difference between the present solution and Murman's SPO result of Ref. 29 cannot be completely resolved with certainty, we should compare our result with the corresponding solution by the time-dependent method of Magnus and Yoshihara,[27] which is available, however, only for the case of a circular-arc airfoil in a slight supersonic free stream ($K_c = -1.829$).

For this purpose, a line OSR procedure with shock fitting is applied to the case just mentioned, using a uniform grid $\Delta\tilde{x} = 0.05$ and $\Delta\tilde{y} = 0.10$. Shock fitting for the bow shock in this case is relatively simple in that $\tilde{\phi} = 0$ everywhere upstream of the shock, which also eliminates the need for a far-field description. With $\tilde{\phi} = 0$ everywhere as an input (trial solution), the bow shock of Magnus and Yoshihara[27] is recovered (to 1% accuracy) in 240 iterations. The results for the bow shock and the sonic boundary are shown in Fig. 16. The subsonic flow region in this case is unaffected by the presence of the portion of shock beyond the sonic downstream point. The shock/sonic boundary can therefore be determined from shock fitting which treats strictly a supersonic-subsonic transition. A single-sweep procedure treating supersonic-supersonic transition (cf. Addendum A.4) has also been used to continue the solution beyond the sonic boundary, yielding results in agreement with those of Ref. 27. Since the bow shock captured by Murman's SPO solution (Ref. 29) compared also quite well with Magnus and Yoshihara's

(27), one sees that the SPO and shock fitting methods do agree in this case. But the shock-fitting method yields far superior resolution in shock location and in the pressure signature, and is therefore much suited for sonic-boom and caustic studies.

One obvious questions remains. Namely, can the line SOR procedure with shock fitting be accelerated? The answer is an affirmative one. We have applied a second-order cyclic acceleration technique to the above mentioned procedure, and succeeded in recovering the bow shock of Fig. 16 (to within 1%) in 64 iterations.

REFERENCES

1. Forsythe, G.E. and Wasow, W.R., Finite-Difference Methods for Partial Differential Equations, John Wiley & Sons, New York, 1960.
2. Young, D., Iterative Solutions for Large System of Linear Equations, Academic Press, New York, 1971.
3. Varga, R.S., Iterative Matrix Analysis, Prentice-Hall, Englewood Cliffs, New Jersey, 1962.
4. Wilkinson, J.H., The Algebraic Eigen-value Problem, Clarendon Press, Oxford, 1965.
5. Isaacson, E. and Keller, H. B., Analysis of Numerical Methods, John Wiley & Sons, Inc., New York, 1966.
6. Dorr, F.W.,"The Direct Solution of the Discrete Poisson Equation On a Rectangle", SIAM Review, vol. 12, no. 2, pp. 248-263, 1970.
7. Roache, P.J., Computational Fluid Dynamics, Hermosa Publishers, P.O. Box 8172, Albuquerque, New Mexico, 1972.
8. Lomax, H. and Steger, J.L., "Relaxation Method in Fluid Mechanics", Annual Review of Fluid Mechanics, vol. 7, Jan. 1975.
9. Fadeev, D.K. and Fadeeva, V.N., Computational Methods of Linear Algebra (translated by R.C. Williams) W.H. Freeman & Co., San Francisco, 1963.
10. Martin, E.D. and Lomax, H. "Rapid Finite Difference Computation of Subsonic and Transonic Aerodynamic Flows", AIAA paper No. 74-11, 1974.
11. South, J.C., Jr., and Jameson, A., "Relaxation Solutions for Inviscid Axisymmetric Transonic Flow over Blunt or Pointed Bodies", in Proceedings AIAA Computational Fluid Dynamics Conference, Palm Springs, Calif., July 19-20, 1973, pp. 8-17.
12. Jameson, A.,"Numerical Calculation of the Three Dimencional Transonic Flow over a Yawed Wing", Proceedings AIAA Computational Fluid Dynamics Conference, pp. 18-26.
13. Cheng, H.K. and Hafez, M.M., "Equivalence Rule and Transonic Flows Involving Lift", Univ. So. Calif. School of Eng. Report USCAE 124, 1973.
14. Sells, C.C.L., "Plane Subcritical Flow Past a Lifting Airfoil", RAE TR-67146, Royal Aircraft Establishment, June 1967.
15. Murman, E.M. and Cole, J.D., "Calculation of Plane Steady Transonic Flow", AIAA Jour., vol. 9, no. 1, 1971, pp. 114-121.
16. Krupp, J.A. and Murman, E.M., "Computation of Transonic Flows Past Lifting Airfoils and Slender Bodies", AIAA Jour., vol. 10, no. 7, 1972, pp. 880-886.
17. Bailey, F.R. and Steger, J.L., "Relaxation Techniques for Three Dimensional Transonic Flow about Wings", AIAA Jour., vol. 11, no.3, 1973, pp. 318-325.
18. Newman, P.A. and Klunker, E.B., "Computation of Transonic Flow about Finite Lifting Wings", AIAA Jour., vol. 10, No. 7, 1972, pp. 971-973.
19. Garabedian, P.R. and Korn, D.G., "Numerical Design of Transonic Airfoils", in Numerical Solution of Partial Differential Equations - II, Academic Press, 1971.
20. Yoshihara, Y., "A Survey of Computational Methods for 2D and 3D Transonic Flows with Shocks", GDCA-ERR-1726, Dec. 1972, Convair Aerospace Div., General Dynamics, San Diego, California.
21. Nieuwland, G.Y. and Spee, B.M., "Transonic Airfoils: Recent Developments in Theory, Experiment and Design", Annual Review of Fluid Mechanics, vol. 5, 1973, pp. 119-150.
22a. Berndt, S.B. and Sedin, Y.C., "A Numerical Method for Transonic Flow Fields", ICAS paper No. 70-13, September 1970.
22b. Sedin, Y. C-J, "Axisymmetric Sonic Flow Computed by a Numerical Method Applied to Slender Bodies, AIAA paper 74- , 1974.
23. Barnwell, R.D., "Numerical Results for the Diffraction of a Normal Shock Wave by a Sphere for the Subsequent Transient Flow", NASA TR R-268, Sept. 1967.
24. Moretti, G., "Thoughts and After Thoughts about Shock Computations", PIBAL Report No. 72-37, Polytechnic Inst. Brooklyn, December 1972.
25. Grossman, B. and Moretti, G., "Time-dependent Computation of Transonic Flows", AIAA paper 70-1322, Houston, Texas, 1970.
26. Moretti, G., "Parametical Analysis of Discretization Procedures for Initial and Boundary-value Problems in Gas Dynamics and their Influence on Accuracy -- Or, Look Ma, No Wiggles!", Polyt. A.E./A.M. Report no. 74-15, Sept. 1974.
27. Magnus, R.M. and Yoshihara, H., "Steady Inviscid Flow over Planar Airfoils - A Search for a Simplified Procedure", NASA CR-2186, Jan. 1973.
28. Magnus, R.M. "The Direct Comparison of the Relaxation Method and the Pseudo-Unsteady Finite Difference Method for Calculating Steady Planar Transonic Flow", TN-73-SP03, General Dynamics, Convair Aerospace Div., San Diego, Calif., 1973.
29. Murman, E.M. "Analysis of Embedded Shock Waves Calculated by Relaxation Methods", AIAA Jour., vol. 12, no. 5, pp. 626-633.
30. Shanks, D., "Nonlinear Transformations of Divergent and Slowly Convergent Sequences", Studies of Applied Math, (J. Math. Phys.), no. 34, pp.1-42, 1955.
31. Aitken, A.C. "On Bernoulli's Numerical Solution of Algebraic Equations', Proc. Royal Society Edinburgh, vol 46, 1926, pp.289-305.
32. Aitken, A.C.,"Studies in Practical Mathematics II, Proc. Royal Soc. Edinburgh, vol. 57, 1937, pp. 269-304.
33. Henrici, P., Elements of Numerical Analysis, John Wiley & Sons, New York, 1964.
34. Van Dyke, M.D. , Perturbation Methods in Fluid Mechanics, Academic Press, New York, 1964.
35. Van Dyke, M.D., "Analysis and Improvement and Perturbation Series", Quart. Jour. Mech. Appl. Math., Nov. 1974.
36. Van Tuyl, A.H. "Calculation of Nozzle Using Padé Fractions", AIAA Jour. vol. 11, no. 4, 1973, pp. 537-541.

37. Cabannes, H., and Bausset, M., "Application of the Method of Padé to the Determination of Shock Waves", in Problems of Hydrodynamics and Continuum Mechanics, in Honor of L.I. Sedov, English ed. published by SIAM, 1968, pp. 95-114.
38. Padé, H., "Sur la representation approchée d'une fonction par des rationelles"Ann. École Nor (3), Supplement, 1892, pp.1-93.
39. Wynn, P., On the Convergence and Stability of Epsilon Algorithm, SIAM Jour. Numerical Anal. vol. 3, 1966, pp. 91-122.
40. Gragg, W.B., "The Padé Table and Its Relation to Certain Algorithms of Numerical Analysis", SIAM Review, vol. 14, no. 1, 1972.
41. Baker, G.A., Gammel, J.L. and Willis, J.G. "An Investigation of the Applicability of the Pade Approximation Method" , Jour. Math. Anal. vol. 2, 1961, pp. 405-418.
42. Lyusternik , L.A., Trudy, Mat. Inst., Steklov, vol. 20, 1947, pp. 44-64.
43. Bellman, R., Introduction to Matrix Analysis, McGraw Hill, New York, 1960.
44a. Roesner, K. private communication.
44b. Nieuwland, G.Y., Transonic Potential Flow around a Family of Quasi-Elliptical Aerofoil Sections, National Aerospace Lab. NLR Tech. Report T. 172 (undated).
45. Forsythe, G.E., "Solving Linear Equations Can be Interesting", Bull. Am. Math. Soc., vol. 59, no. 4, 1953, pp. 309-310.
46. Forsythe, G.E., "Tentative Classification of Methods and Bibliography on Solving Systems of Linear Equation", in Simultaneous Linear Equations and the Determination of Eigenvalues Nat. Bur. Stand., Appl. Math. Series 29, 1953 p. 7, Item 21b2.
47. Jameson, A., "Solution of Transonic Flows over Airfoils and Wing Including Flows at Mach 1", to appear in Comm. Pure Appl. Math.
48. Newman, P.A. and Davis, R.M., "Imput Description for Jameson's 3-D Transonic Airfoil Analysis Program", NASA Tech. Memo. X-71919, Feb. 1974.
49. Brant, A., "Multi-Level Adaptive Technique (MLAT) for Fast Numerical Solution to Boundary Value Problems", Proc. 3rd Int'l. Conference Numerical Methods in Fluid Mech., Paris, June 1973.
50. Hafez, M.M. and Cheng, H. K., "On Acceleration of Convergence and Shock-Fitting in Transonic Flow Computations", Univ. So. Calif. Memo, 1973.
51. von Kármán, Theodore, "The Similarity Law of Transonic Flow", Jour. Math. and Physics, vol. 26, 1947, p.3.
52. Cole, J.D., "Twenty Years of Transonic Flow", Boeing Scientific Research Lab. Doc. D1-82-0878, 1969.
53 Oswatitsch, K. and Zierep, J., "Das Problem des Senkrechten Stossen an Einer Gekrümmten Wand", ZAMM, vol. 40, Suppl. 1960, pp. T 143-144.
54. Ferrari, C. and Tricomi, F.G. , Transonic Aerodynamics, Academic Press, New York, 1968.
55. Knechtel, E.D., "Experimental Investigation at Transonic Speeds of Pressure Distributions over Wedge and Circular - Arc Airfoil Sections and Evaluations of Perforated-Wall Interference", NASA TN D-15, 1959.
56. Garabedian, P.R., "Estimation of the Relaxation Factor for Small Mesh Size", Math. Tables Aids Comput., vol. 10, pp. 183-185, 1956.
57. Young, D.M., "Iterative Solution of Linear and Nonlinear Systems derived from Elliptic Partial Differential Equations", Center for Numerical Analysis Univ. of Texas at Austin Report CNA-93, 1974.
58. Della Torre, E. and Kinsner, W., "Convergence Properties of the Successive Extrapolation Relaxation (S.E.R.) Method, J. Inst. Maths. Applics, vol. 12, 175-185, 1973.

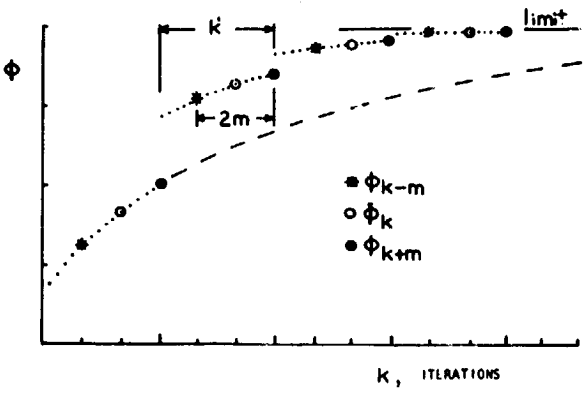

Fig. 1 Cyclic acceleration technique applied to an iterative solution, illustrated for the first-order transform. The cycle is repeated every k' iteration.

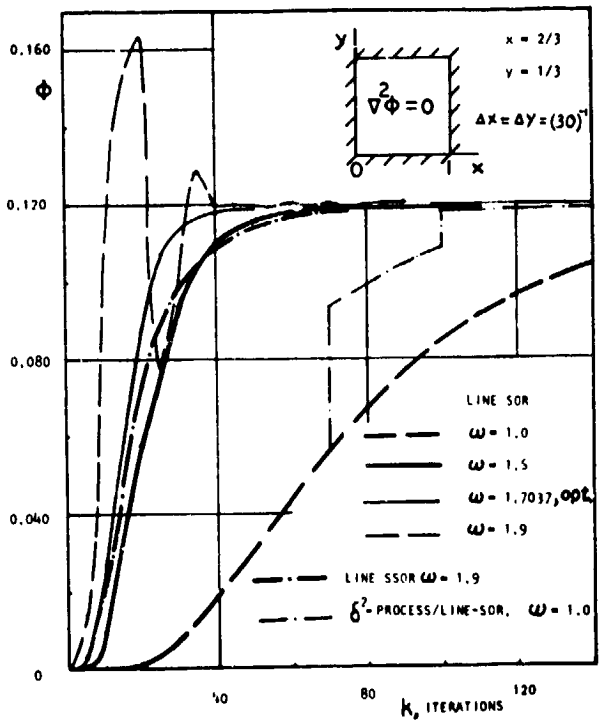

Fig. 2 Convergence history of a line SOR solution to a model Dirichlet problem for different values of relaxation parameter. Also included is a case with reverse sweep (line SSOR) and a case accelerated by the δ^2 - process (applied to every grid point).

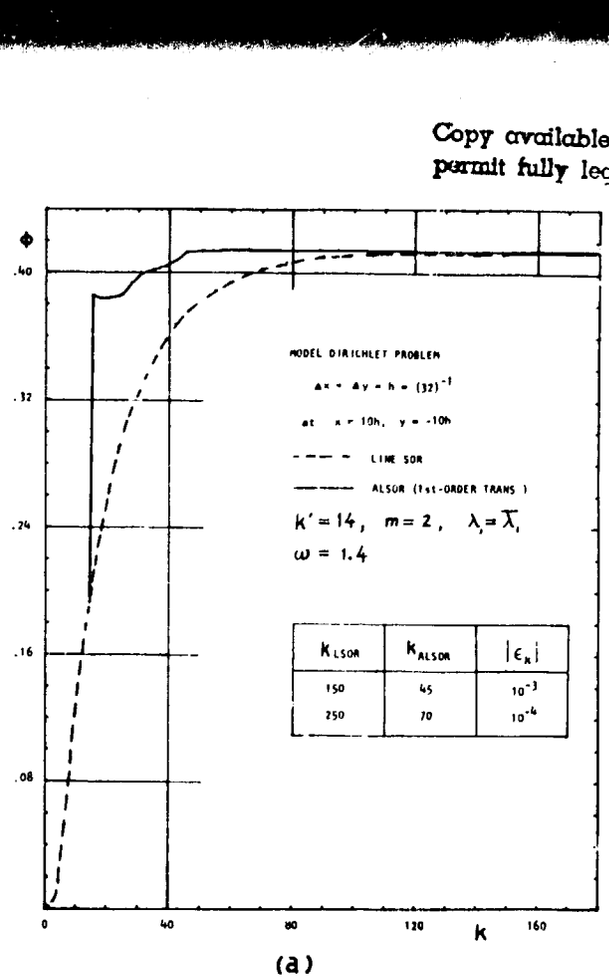

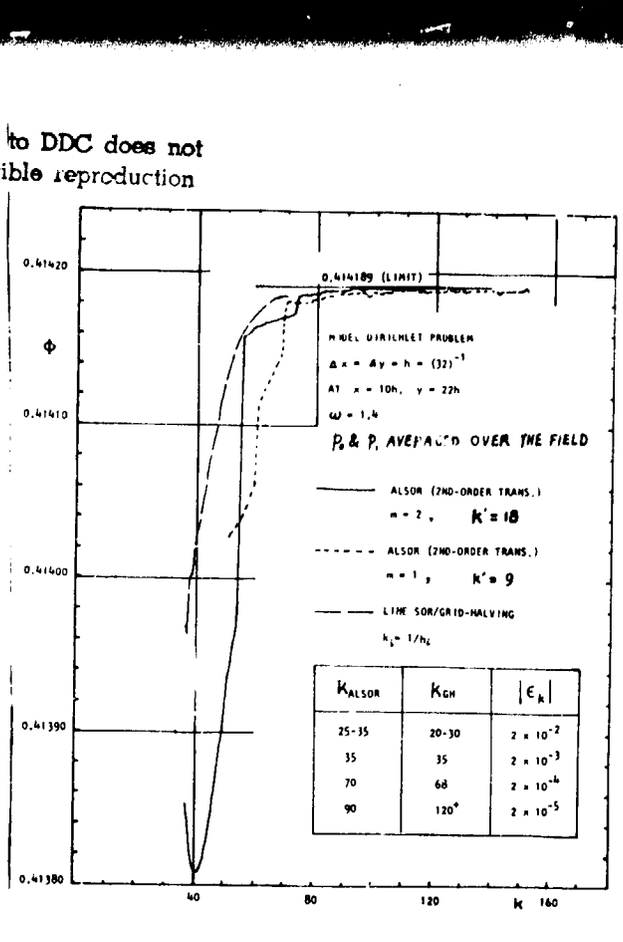

Fig. 4 Test of cyclic acceleration technique on a line SOR solution to a model Dirichlet problem, using second-order transform. Aiso included is the convergence history of a solution using grid-refinement technique.

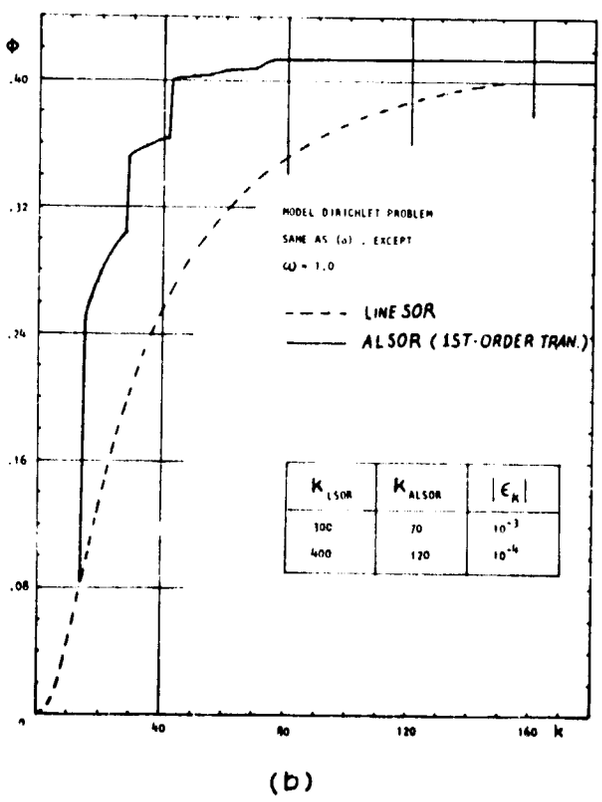

Fig. 3 Test of cyclic acceleration technique on a line SOR solution to a model Dirichlet problem, using first-order transform: (a) $\omega = 1.4$, (b) $\omega = 1.0$.

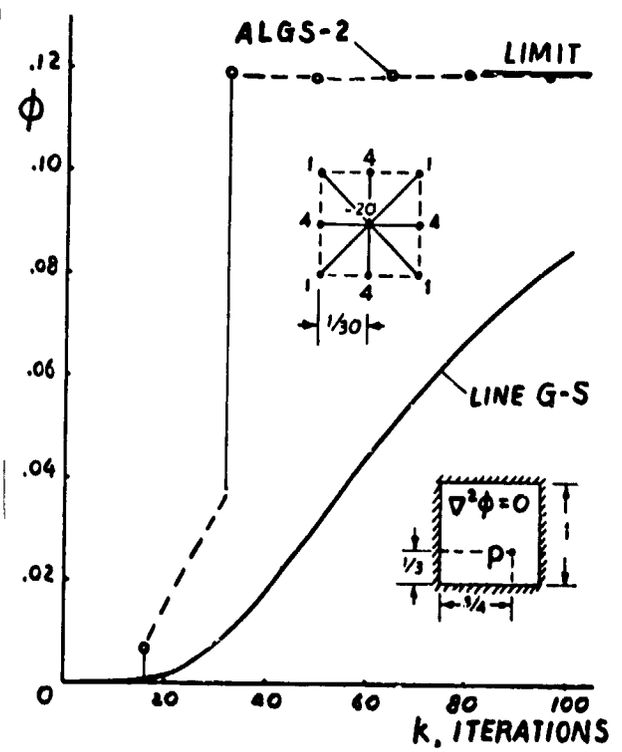

Fig. 4.A Test of second-order cyclic acceleration technique on a line Gauss-Seidel procedure based on a 9-point central difference scheme for a model Dirichlet problem.

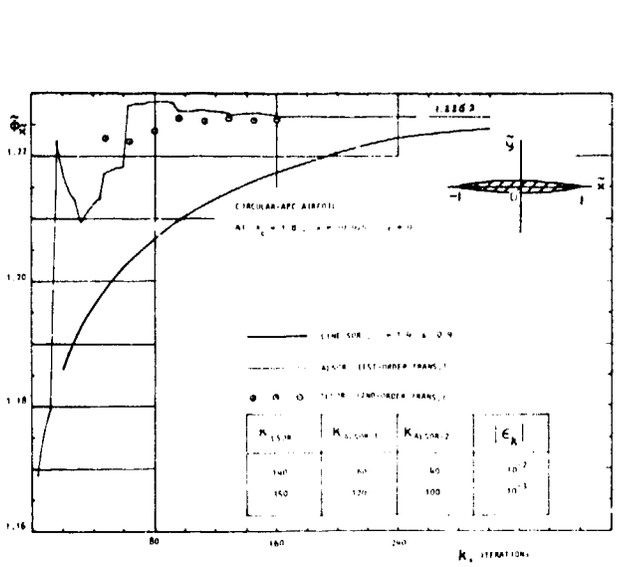

(a)

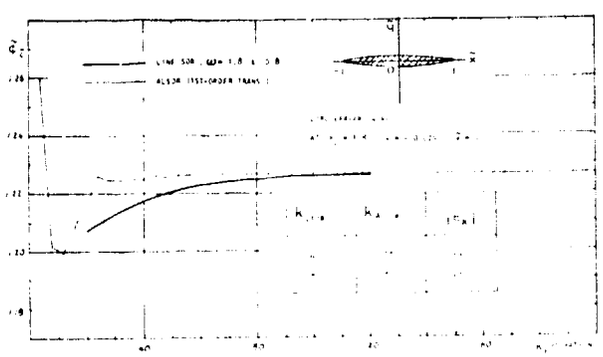

(b)

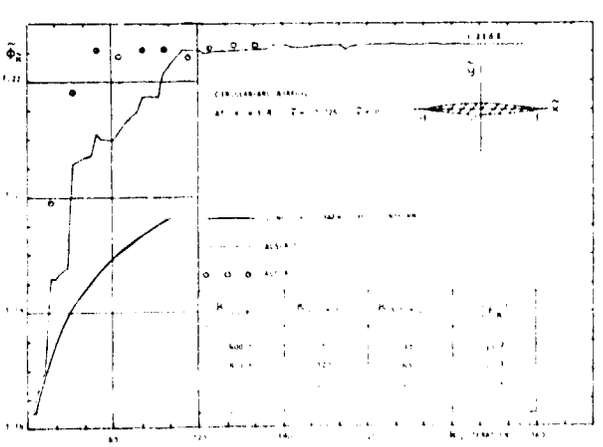

(c)

Fig. 5 Test of cylic acceleration technique on line SOR solution to a supercritical transonic flow over a circular-arc airfoil at zero incidence with $K_c = 1.8$, using first and second order transforms: (a) $\omega = 1.4$ and 0.9, (b) $\omega = 1.8$ and 0.8, (c) $\omega = 0.95$, uniform.

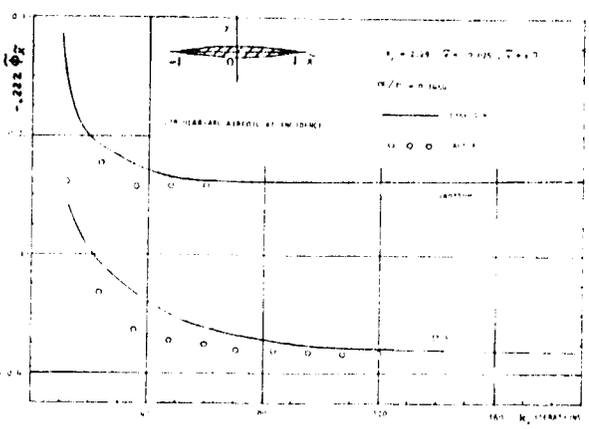

(a)

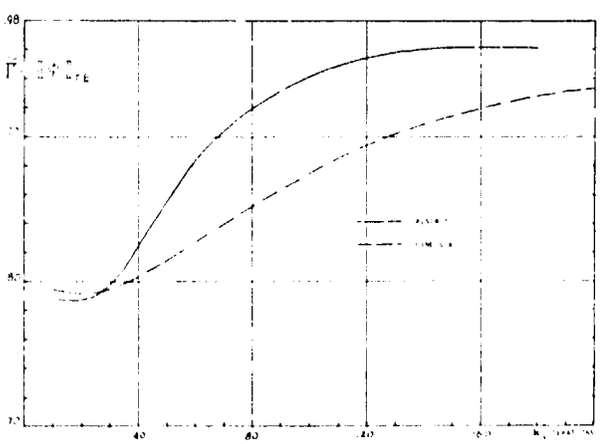

(b)

Fig. 6 Test of cylic acceleration technique on line SOR solution with $\omega = 1.8$ and 0.8 to a supercritical transonic flow over a circular-arc airfoil at incidence with $K_c = 1.8$, $\alpha/\tau = 0.1454$, using first-order transforms: (a) convergence history of surface speed near midchord $\tilde{x} = -0.025$, $\tilde{y} = \pm 0$, (b) convergence history of the circulation.

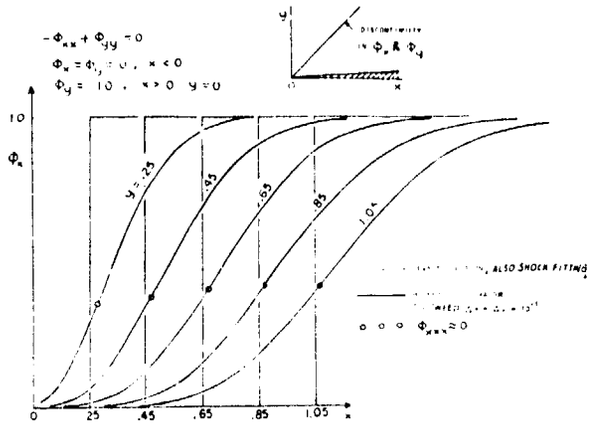

Fig. 7 Illustration of shock transition profiles in a linear supersonic flow, using hyperbolic difference operator.

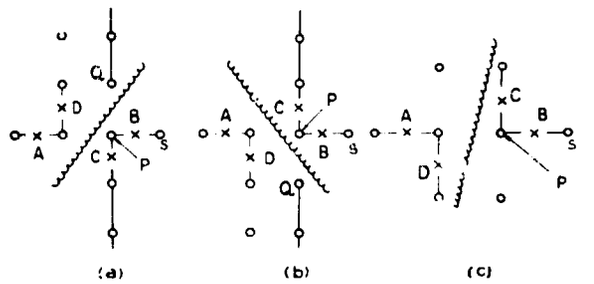

Fig. 8 Grid-point arrangements and shock inclinations in shock-fitting method.

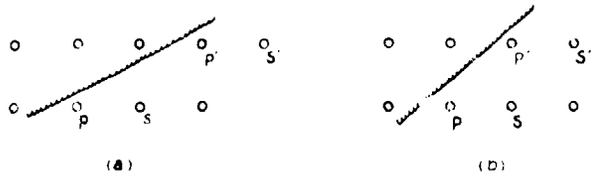

Fig. 8.A Grid point arrangements for shock fitting in cases of supersonic-supersonic transitions.

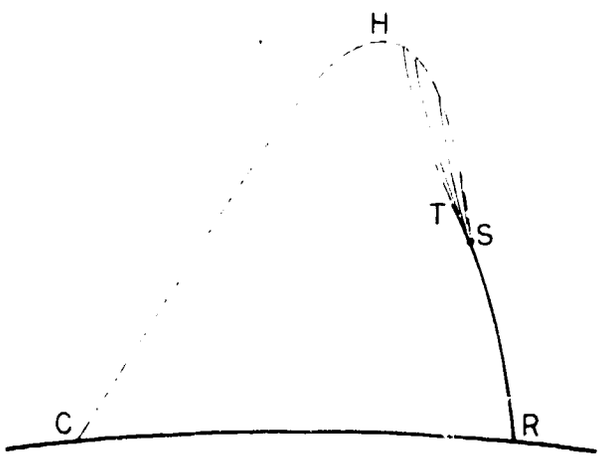

Fig. 9 Illustration of shock/sonic boundary delimiting the embedded supersonic region.

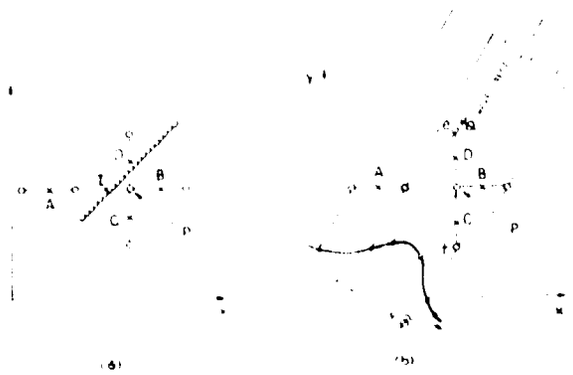

Fig. 10 Description for shock-point operator (SPO): (a) grid configuration in the SPO, (b) SPO treating a shock profile as a continuous solution.

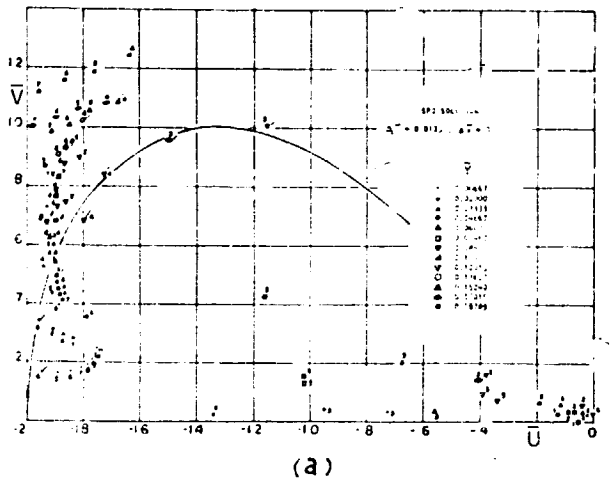

(a)

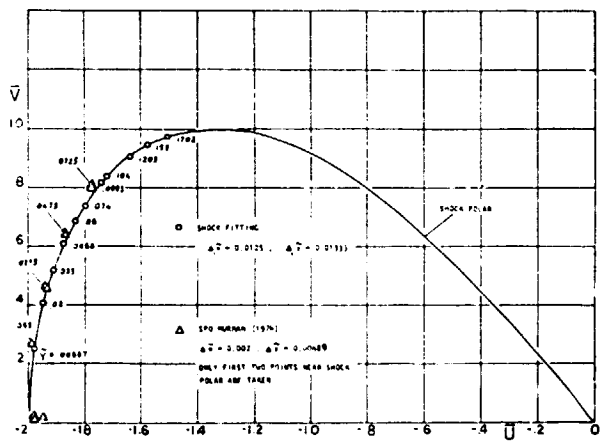

(b)

Fig. 11 Circular-arc airfoil at $K_c = 1.8$. Comparison with hodograph shock polar for the same grid: (a) SPO, (b) Shock-fitting.

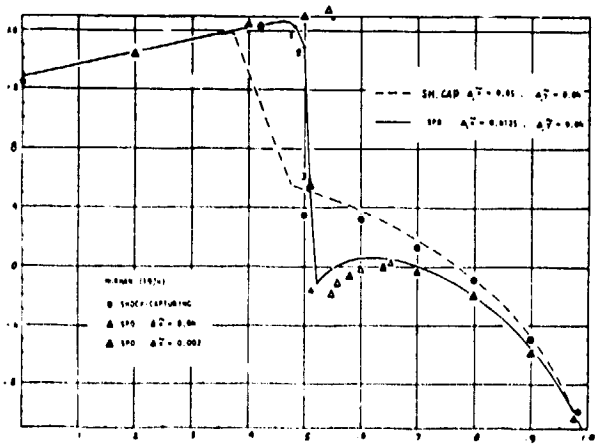

Fig. 12 Surface velocity over a circular-arc airfoil at $K_c = 1.8$ for $\Delta_1\tilde{x} = 0.0125$, $\Delta_1\tilde{y} = 0.0133$: Comparison of programs (ii), programs (iii), the non-conservative and fully conservative programs of Murman (AIAA 1974).

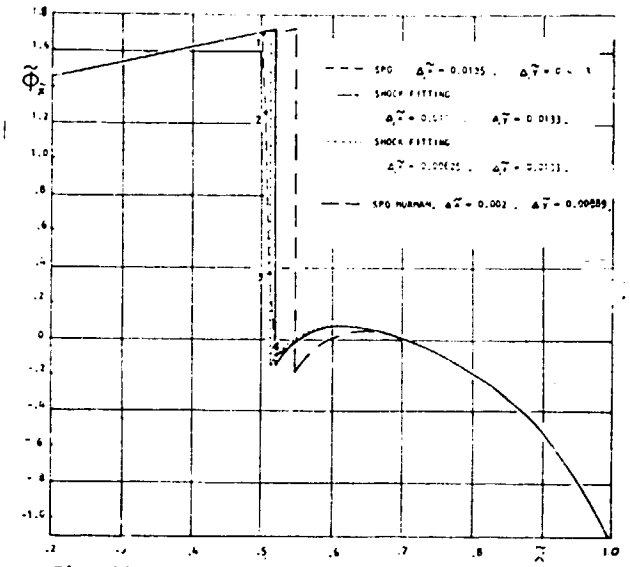

Fig. 13 Surface velocity over a circular-arc airfoil at $K_c = 1.8$ for $\Delta_1\tilde{x} = 0.0125$, $\Delta_1\tilde{y} = 0.0133$: Comparing SPO and shock-fitting. Results from grid-halving ($\Delta_1\tilde{x} = 0.00625$) and data from Ref. 29 are also included.

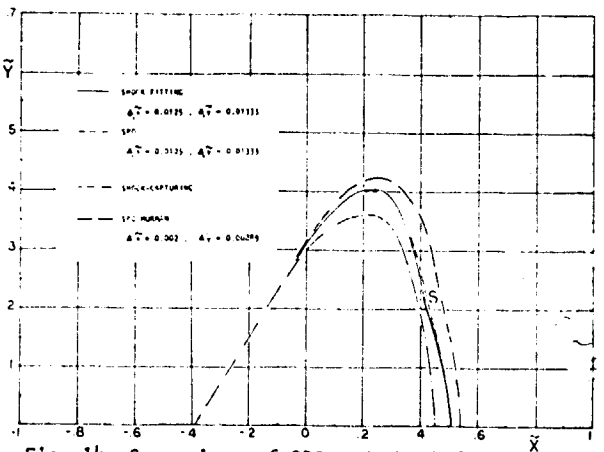

Fig. 14 Comparison of SPO and shock-fitting results for sonic/shock boundary above a circular-arc airfoil at $K_c = 1.8$ for $\Delta_1\tilde{x} = 0.0125$, $\Delta_1\tilde{y} = 0.0133$. Data inferred from SPO result from Murman (AIAA 1974) and from a shock-capturing solution are also included.

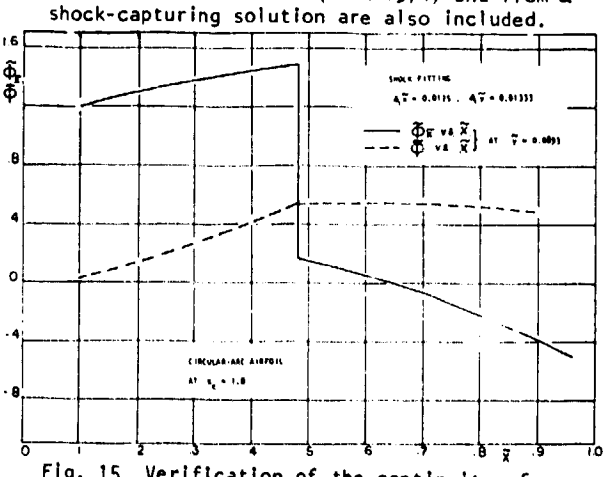

Fig. 15 Verification of the continuity of velocity potential across shock.

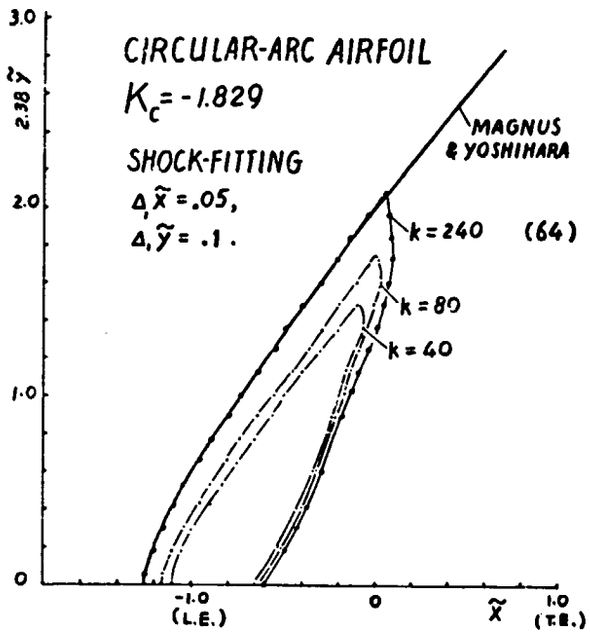

Fig. 16 Comparison of shock-fitting and pseudo-unsteady methods for the shock/sonic boundary over a circular-arc airfoil at $K_c = -1.829$, with uniform mesh $\Delta\tilde{x} = 0.05$, $\Delta\tilde{y} = 0.10$. Note that the accelerated shock fitting yields results indistinguishable from the unaccelerated one in 64 iterations.